Research Square

Preprints are preliminary reports that have not undergone peer review.
They should not be considered conclusive, used to inform clinical practice,
or referenced by the media as validated information.

Uncertainty-weighted fuzzy clustering disentangles climate-stress VOC fingerprints and associated stress-dependent temperature sensitivity in urban trees

Biplob Dey
Institute of Climate and Energy Systems: Troposphere (ICE-3), Forschungszentrum Jülich
Clémence Depp
Institute of Climate and Energy Systems: Troposphere (ICE-3), Forschungszentrum Jülich
Yichen Gu
Institute of Climate and Energy Systems: Troposphere (ICE-3), Forschungszentrum Jülich
Anna Novelli
Institute of Climate and Energy Systems: Troposphere (ICE-3), Forschungszentrum Jülich
Hendrik Fuchs
Institute of Climate and Energy Systems: Troposphere (ICE-3), Forschungszentrum Jülich
Thorsten Hohaus
Institute of Climate and Energy Systems: Troposphere (ICE-3), Forschungszentrum Jülich
Eva Y. Pfannerstill
e.pfannerstill@fz-juelich.de

Institute of Climate and Energy Systems: Troposphere (ICE-3), Forschungszentrum Jülich

Article

Keywords:

Posted Date: November 13th, 2026

DOI: https://doi.org/10.21203/rs.3.rs-11564917/v1

License: This work is licensed under a Creative Commons Attribution 4.0 International License.
Read Full License

Additional Declarations: No competing interests reported.

Uncertainty-weighted fuzzy clustering disentangles climate-stress VOC fingerprints and associated stress-dependent temperature sensitivity in urban trees

Biplob Dey[1,3], Clémence Depp[1,2], Yichen Gu[1], Anna Novelli[1], Hendrik Fuchs[1,4], Thorsten Hohaus[1], Eva Y. Pfannerstill[1,2,*]

[1]Institute of Climate and Energy Systems: Troposphere (ICE-3), Forschungszentrum Jülich, Jülich, Germany
[2]Institute of Geophysics and Meteorology, University of Cologne, Cologne, Germany
[3]Bioclimatology, Faculty of Forest Sciences and Forest Ecology, University of Göttingen, Göttingen, Germany
[4]Department of Physics, University of Cologne, Cologne, Germany

Correspondence: Eva Y. Pfannerstill (e.pfannerstill@fz-juelich.de)

Abstract

Climate change increases the severity and frequency of heat and oxidative stress that plants experience, yet their simultaneous effects on biogenic volatile organic compounds (BVOCs) emissions remains poorly understood, complicating the predictability of future air quality and climate. Here, canopy BVOC emissions from linden and chestnut trees were measured over a continuous two-month chamber experiment without stress, heat stress, and combined O_3 and heat stress. To untangle stress-associated BVOC fingerprints, we developed an unsupervised uncertainty-weighted fuzzy c-means (UWFCM) algorithm that directly incorporates compound- and measurement-specific analytical uncertainties into clustering.

UWFCM identified monoterpenes (increased up to 3-fold) and sesquiterpenes (up to 22-fold) as the primary heat-stress markers in both species, while increased diterpenes characterized combined O_3 and heat stress in linden. Stress-induced *de novo* emissions resulted in carbon loss up to ~14% of net daytime carbon fixation, a substantial stress-related carbon reallocation. The temperature sensitivity of terpenoid emissions was strongly stress-dependent. These findings have important implications for global BVOC parameterizations, estimates of daytime NO_x-driven ozone chemistry and secondary organic aerosol formation under future climate extremes.

Introduction

Forest ecosystems are considerably affected by the increasing frequency and severity of climate extremes[1] and are projected to experience more extreme events throughout the 21st century[2,3], particularly in Europe[4]. Heatwaves, droughts and elevated near-ground ozone are increasingly converging into complex stress events, particularly in urban and peri-urban forests where increased concentrations of anthropogenic emissions coincide with elevated temperatures[5–8]. These disturbances can substantially alter ecosystem productivity, carbon sequestration, and vegetation-atmosphere interactions, thereby affecting both local air quality and regional climate[8–10].

One of the primary physiological responses to environmental stress is the emission of biogenic volatile organic compounds (BVOCs)[11], which function not only as protective metabolites but also as signaling molecules[12]. For example, under heat stress, plants can increase isoprene emissions to improve thermotolerance[13]. Ozone exposure can induce sesquiterpene emissions[14], as sesquiterpenes rapidly react with ozone and may thereby contribute to protection against oxidative stress[15]. Although only a small fraction of the total assimilated carbon is re-emitted as VOCs[16], these emissions have far-reaching consequences. Upon release, they become a key player in atmospheric chemistry due to their high reactivity with atmospheric oxidants, contributing to the formation of secondary organic aerosols (SOA), cloud condensation nuclei, and ozone[8,17,18]. Therefore, characterizing BVOC emissions under complex stress is essential for both ecosystem and atmospheric models.

Despite decades of research on biogenic VOC emissions, important uncertainties exist regarding how vegetation responds to sequential and interacting climate stressors. Most experimental and field studies have focused on individual stress events, including heatwaves[19–23], drought[20,24], ozone exposure[14,25], herbivory[26–28] and large-scale climate anomalies such as El

Niño[29–31], and have primarily characterized responses through changes in emission rates, isoprenoid speciation and their role to characterize the stress, or a limited number of stress-marker compounds. These studies have demonstrated that environmental stress can alter the emissions of isoprene[32,33], monoterpenes[23], sesquiterpenes[14], and oxygenated VOCs[32,34] through fundamental physiological processes, including oxidative stress, membrane damage, defense signaling, and secondary metabolism[12,29,31]. Recent studies further indicate that stress can induce the formation of oxygenated monoterpenes and sesquiterpenes during stress adaptation and recovery[29]. However, environmental stress rarely occurs in isolation[35]. As heatwaves often coincide with elevated ozone levels due to photochemical ozone formation[36], vegetation is exposed to combined heat-ozone stresses whose effects may differ substantially from the individual stressors.

Advances in proton-transfer-reaction time-of-flight mass spectrometry (PTR-ToF-MS) enable online measurements of hundreds of volatile compounds with unprecedented chemical complexity. Individual VOCs originate from multiple biosynthetic pathways[11,32,37], differ substantially in volatility and atmospheric reactivity[38], and are associated with compound- and concentration-dependent measurement uncertainties[39]. Consequently, biologically meaningful stress responses can be difficult to distinguish from background noise (e.g., fluctuations in ion counts and residual background ions) and analytical variability (e.g., changes in ionization efficiency, instrument sensitivity). Complex VOC datasets are commonly explored using multivariate approaches, including dimensionality-reduction techniques (for example, principal component analysis[40,41]), and source-apportionment frameworks like positive matrix factorization[42,43]. Unsupervised machine learning methods, such as fuzzy c-means clustering[44], offer a complementary approach to identifying patterns in complex timeseries or VOC datasets.

Positive matrix factorization resolves additive, time-invariant source profiles whose contributions change in time, and answers how much of the measured signal each source contributes. It can incorporate measurement uncertainty explicitly, and its factors are constrained to be non-negative and additive. Plant stress-induced VOC emissions often originate from interconnected biosynthetic pathways[45], show overlapping temporal responses[32] and evolve dynamically as stress progresses. So, a compound may reasonably belong in part to a constitutive emissions pattern and in part to a stress pattern at the same time. Fuzzy clustering can represent exactly that, through weighted membership. PMF reconstructs a signal statistically, while fuzzy c-means looks for temporal co-behavior and is therefore better suited for compounds emitted from the same source with changing temporal behavior. But conventional fuzzy c-means weights every measurement equally and has no mechanism for compound and observation specific analytical uncertainty. Integrating these uncertainties into the clustering process as a novel approach, we strive to reduce the influence of less reliable measurements, and more robust identification of stress-associated emission patterns and fingerprints.

Stress-related VOC emission changes increase the uncertainty in atmospheric chemistry model predictions. Current BVOC emission frameworks, including MEGAN (Model of Emissions of Gases and Aerosols from Nature), use fixed temperature-response functions within plant functional types[46,47]. However, recent studies show that temperature sensitivities vary substantially among ecosystems[48] and are strongly modified by co-occurring environmental drivers, rather than temperature alone[49]. Incorporating such stress-dependent temperature sensitivities into BVOC emission models may improve predictions of emissions and their atmospheric impacts under future climate extremes.

Here, we combined controlled sequential heat and ozone stress experiments with emission sampling from the canopy of two tree species that were chosen for their frequent application in climate-adapted urban greening[50], linden (*Tilia cordata*) and chestnut (*Castanea sativa*). We first quantified stress-induced shifts in VOC emissions and the assimilated carbon loss associated with those emissions. Then we newly introduced an unsupervised machine learning algorithm, uncertainty-weighted fuzzy clustering (UWFCM), to resolve stress-specific VOC fingerprints while explicitly incorporating uncertainty-derived weighting functions in the source-apportionment process. Finally, we evaluated how stress modifies the temperature sensitivities of major fingerprint compounds, including monoterpenes, sesquiterpenes, and diterpenes. Together, these results show how multi-stress reshapes carbon dynamics, VOC fingerprints and their temperature sensitivity, providing comprehensive insights for BVOC emission parameterizations and transferable uncertainty-aware algorithms for source-apportionment, interpreting complex mass spectrometric data and ecosystem data analysis.

Results

Climate stress reshaped carbon dynamics

To understand how heat and combined heat-ozone stress affected BVOC emissions from trees, emissions were quantified (Fig.1). While the effects of stress on tree physiology have been extensively investigated elsewhere[25,51], in this study CO_2 exchange was monitored to assess changes in photosynthetic carbon uptake and respiratory activity as a stress indicator, whereas methyl salicylate (MeSa; $C_8H_9O_3^+$; m/z 153.05) emissions were used as a proxy for stress-associated signalling[52] molecules. Before stress, both linden and chestnut showed distinct diel CO_2 exchange characterized by strong daytime CO_2 uptake (due to photosynthesis) and nighttime release (respiration), consistent with active daytime carbon sink behavior (Supplementary information, Fig. S1). Subsequent stress exposure showed that daytime CO_2 uptake declined substantially in chestnut under heat and combined ozone-heat periods, whereas linden maintained CO_2 uptake similar to pre-stress levels. The decline in chestnut photosynthetic activity is consistent with documented heat-induced photosynthetic inhibition[51]. In contrast, linden maintained daytime CO_2 uptake despite higher VOC carbon emissions than chestnut during heat stress (46.9 versus 24.4 nmol C m^{-2} s^{-1}; Fig. 1f). Chestnut's uptake collapsed by about two-thirds while its VOC carbon emission rose 2.5-fold. A previous study[53] on linden has showed adjustments in the photosynthetic temperature optimum under warmer conditions, but that does not necessarily mean they absorb more CO_2 or maintain their photosynthetic activity.

The reduced carbon assimilation under heat stress (decrease up to ~54%, Fig. S1, Table S1), is likely due to the lower specificity of the carbon fixation enzyme RuBisCO for CO_2 at elevated temperatures[54]. Further inhibition of carbon assimilation observed under combined heat-ozone (Fig.S1) stress may also be consistent with ozone-induced oxidative effects on the Calvin cycle[55] and photosynthetic electron transport through ROS (reactive oxygen species) mediated mechanisms[56], which can limit ATP (adenosine triphosphate) and NADPH (nicotinamide adenine dinucleotide phosphate) production required for carbon fixation[54]. The physiological stress was also accompanied by substantial increases in VOC-associated carbon loss (Fig.1h). During heat stress, episodic daytime VOC carbon loss exceeded ~15% of the net daytime CO_2 uptake in chestnut and 9% in linden (Fig.1h), a major loss of assimilated carbon through volatile emissions as a form of stress compensation[57]. Under combined heat and ozone stress, the relative VOC carbon loss decreased in both species, particularly in linden, despite the MeSa stress signal being at its peak. Concurrent increases in MeSa emissions further indicate signs of oxidative stress during stress exposure (Fig.S1, c-d), consistent with Jardine et al.[58], reporting increased MeSa emissions under heat due to declining photosystem-II efficiency and stress-responsive photosynthetic regulation.

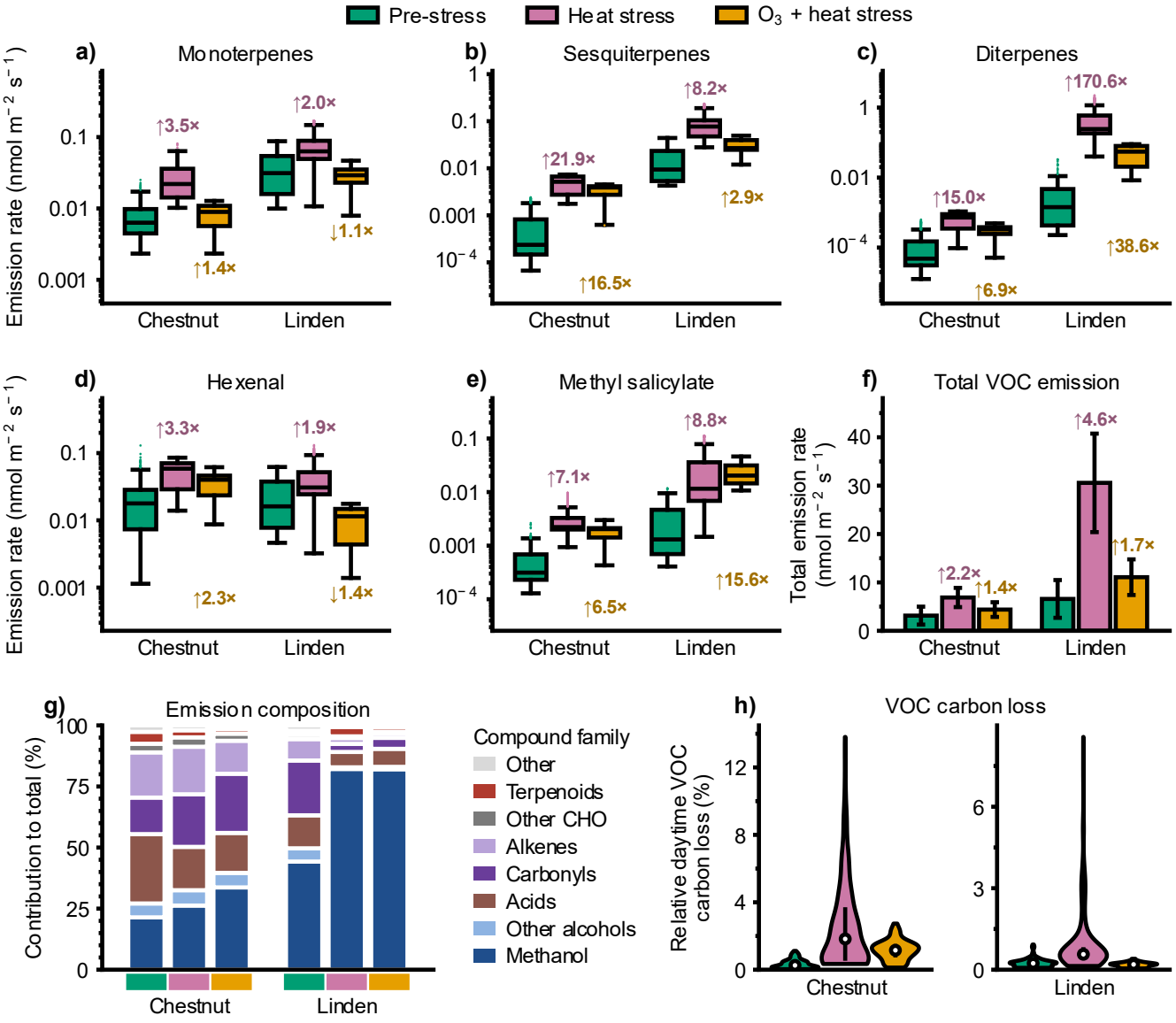


Figure 1 Volatile organic compound emissions and the composition of chestnut and linden under different stress conditions. Subplot (a-e) shows emission rates for major BVOC compounds. Annotations within the subplot indicate fold changes relative to pre-stress conditions. Boxes represent interquartile ranges (IQR), center lines indicate medians, and whiskers represent 1.5× IQR. Subplot (f) shows total BVOC emission rates (mean ± standard deviation) in nmol.m^{-2}.s^{-1} across stress. (g) shows the relative contribution of major compound families. (h) shows *de novo* VOC-carbon loss relative to net daytime CO_2 uptake. This figure presents the absolute emissions. Chestnut emission rates may be underestimated, and their diel variability dampened owing to the inlet artefact (more in methods and supplementary section 04). This does not affect relative changes between conditions.

Stress-driven changes in BVOC emissions

Stress caused substantial increases in constitutive and stress-associated VOC emissions, although the magnitude of the response was species-dependent. The strongest stress-induced responses during heat exposure occurred for terpenoid emissions, with increased emissions of monoterpenes (~3-fold and ~2-fold for chestnut and linden, respectively), and sesquiterpenes (~14-fold and ~8-fold) (Fig.1a-b). These intense terpenoid emissions during heat stress agree with recent chamber[33] and field studies[23,30,59] reporting increased monoterpene and sesquiterpene emissions under elevated temperature.

Beyond these commonly reported compounds, heat stress triggered a particularly strong increase in diterpene ($C_{20}H_{33}^+$, m/z 273.25) emissions (~170-fold in linden and ~8-fold in chestnut; Fig. 1c and Table S2). Atmospheric observations of

diterpenes remain scarce due to analytical challenges, and only a limited number of plant species have been investigated to date[60–62]. Besides *de novo* emission, diterpenes can also be emitted from the storage pools[60,63], and they are temperature-dependent[60] like monoterpenes[48]. Recent studies[60] point out that diterpene emissions are due to highly active secondary metabolism. Against this background, diterpenes may represent a more important component of heat-stress emissions than currently recognized.

In both species, heat stress shifted the emission composition toward oxygenated compounds of short carbon chain length (Fig.1g). Among alcohols, methanol (CH_4O^+, *m/z* 33.033) increased from 24% to 33% of total emission from chestnut and from 44% to 82% from linden, whereas phenolic alcohols such as phenol ($C_6H_7O^+$, *m/z* 95.049) declined. Among carbonyls, chestnut showed a substantial increase in short-chain species, including acetaldehyde ($C_2H_5O^+$, *m/z* 45.034; 13%), $C_4H_7O^+$ (*m/z* 71.049; e.g. MVK/MACR) and $C_4H_9O^+$ (*m/z* 73.065; e.g. methyl ethyl ketone). Attribution of PTR-MS signals at m/z 69.070 ($C_5H_9^+$) by the coupled gas chromatograph (GC) indicated no significant contribution of isoprene to this mass. Heat stress caused a shift of this signal from long-chain towards shorter-chain aldehyde fragments, with declining nonanal (74% to 7%) and increasing pentanal (5% to 41%) contributions (Supplementary Fig. S2c,i). In linden emissions, by contrast, the carbonyl fraction declined (22% to 3%), and acetaldehyde was below the GC detection limit (Fig. S2g). The relative contribution of organic acids (mainly acetic acid) roughly halved in both species (chestnut 27% to 15%, linden 14% to 6%, Fig.1g).

Since the increasing abundance of oxygenated VOCs under heat stress coincided with a decline in net carbon balance, a larger fraction of assimilated carbon appears to be redirected toward stress-response. Shifts towards methanol emissions are consistent with cell wall degradation and remodeling under thermal stress[64], whereas higher acetaldehyde emissions reflect oxidative stress and membrane damage rising from ROS (reactive oxygen species)-driven lipid peroxidation[65]. Heat-induced membrane dysfunction can also result in the release of various compounds such as aldehydes or ethane[57,66].

In contrast to heat alone, ozone addition to the heat stress altered the overall composition of the emissions rather than further amplifying emissions. Although total VOC emissions under combined ozone-heat stress remained above pre-stress conditions in both chestnut (~6 nmol m^{-2} s^{-1}, with the absolute value potentially underestimated due to a sampling setup error, see methods) and linden (~11 nmol m^{-2} s^{-1}), combined stress generally inhibited the strong heat-induced emissions (Fig.1f). Nevertheless, several stress-responsive compounds remained strongly elevated including sesquiterpenes (~16-fold in chestnut, 3-fold in linden), and diterpene (~7-fold in chestnut, 39-fold in linden). This compositional restructuring was accompanied by a pronounced shift toward emissions of oxygenated compounds. In linden emissions, methanol remained dominant (82% of total emissions), whereas the acid (14% to 7%) and carbonyl (22% to 4%) fractions declined substantially relative to pre-stress. These findings from both species indicate that climate stress influenced carbon dynamics not only by reducing carbon assimilation but also by fundamentally altering the chemical fate of assimilated carbon.

Uncertainty-weighted fuzzy clustering resolves temporal cluster dynamics

Ecosystem stress rarely occurs as an isolated event, but rather periodically and simultaneously, which can change emissions dynamically. To address such complex yet overlapping responses, uncertainty-weighted fuzzy clustering (UWFCM) was applied to identify stress-related states while explicitly accounting for the heterogeneous analytical uncertainty across the VOC features. Measurement uncertainties associated with individual PTR-ToF-MS ion signals (mass-to-charge rations (m/z)) were incorporated into the clustering algorithm (see Methods), giving less weight to uncertain measurements when identifying groups of VOCs with similar emission patterns. While uncertainty is often taken into account in statistical source-receptor models like positive matrix factorization, the application of instrumental uncertainty weighting in an FCM approach is, to our knowledge, new.

Before clustering, multiple data transformation techniques were systematically evaluated, and candidate clustering solutions were explored across cluster dimensions from cluster 2 to 10. Fuzziness coefficients between 1.2 and 2.0 using complementary clustering indices, including the fuzzy partition coefficient (FPC), partition entropy (PE), fuzzy silhouette score, etc. (Fig.S3-S4). Although several mathematical indices favored a two-cluster solution, this primarily reflected the

broad separation between stressed and non-stressed emission states and therefore provided limited biological information in the underlying cluster. Consequently, higher-dimensional clustering solutions were further evaluated to determine whether additional stress-related clusters appeared (details discussed in supplementary information section 03).

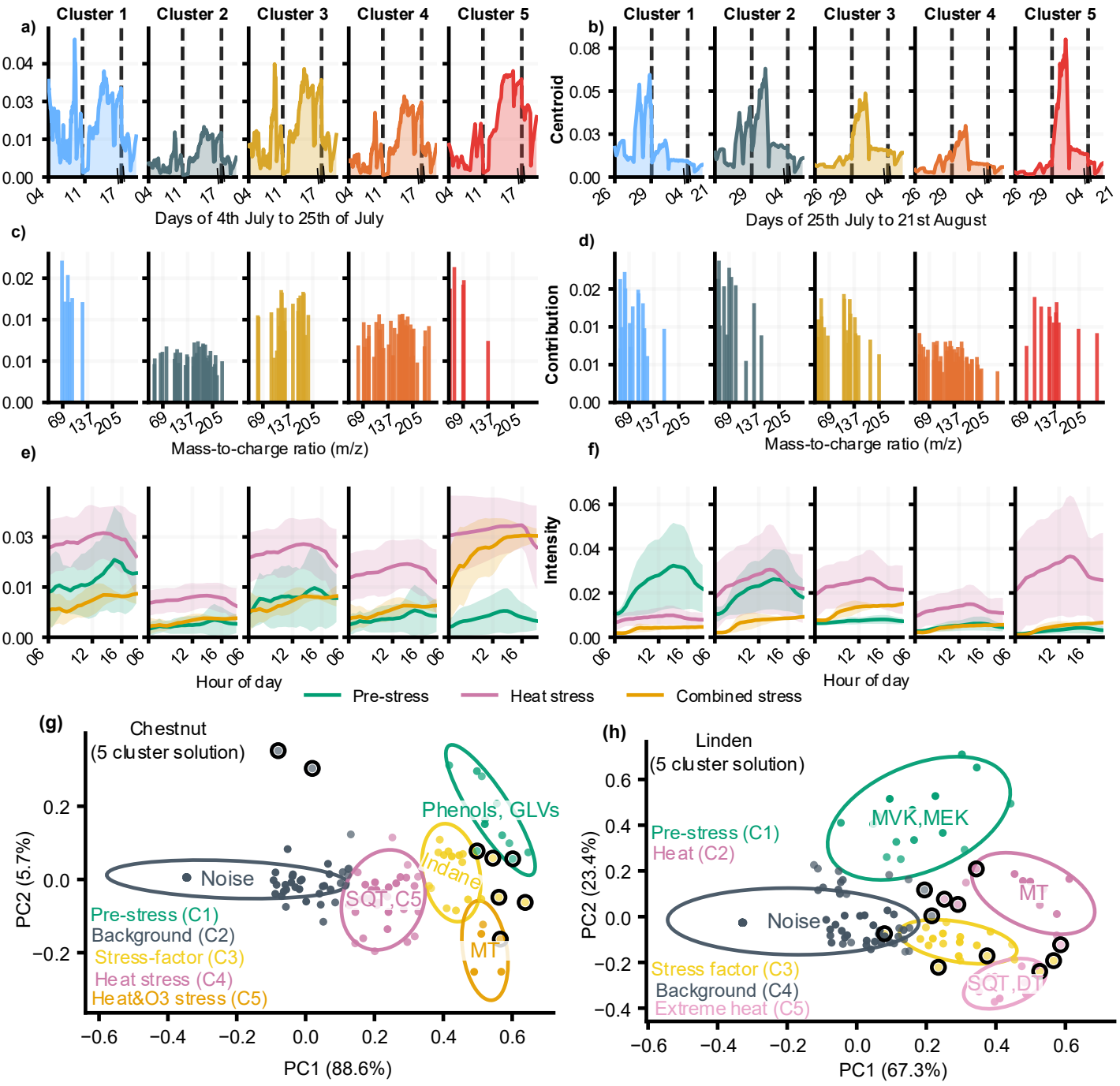


Figure 2 Uncertainty-weighted fuzzy c-means resolved cluster solutions for chestnut (left) and linden (right). Subplots (a–b) show the temporal evolution of the uncertainty-weighted cluster centroids (normalized cluster signals) derived from the transformed VOC emission matrix. Dashed vertical lines indicate transitions between pre-stress, heat stress, and combined heat–ozone stress periods. Subplots (c–d) present the relative contribution of individual VOCs (m/z) to each cluster shown for compounds with membership ≥ 0.5 in that cluster. Subplots (e–f) illustrate the diel behaviour of the normalized cluster signals, lines show the smoothed mean and shaded bands ± standard deviation. Cluster structure was visualized by projecting

the transformed, uncertainty-weighted profiles onto their first two principal components (g–h). PCA was used solely for two-dimensional display and at no point entered the clustering, which was performed in the full temporal space. Ellipses are 2σ covariance ellipses over compounds with membership ≥ 0.5 and are indicative only. C1-C5 corresponds to Clusters 1-5, respectively.

As cluster dimensionality increased, distinct VOC groups associated with terpenoid emissions, oxygenated stress compounds, and signals showing limited stress-dependent variability became more clearly distinguishable. Importantly, cluster evolution remained hierarchically coherent across successive solutions, with major stress-associated emission features persisting consistently rather than fragmenting randomly between clusters (Fig.S5,S7). This persistence indicated that the identified structures reflected biologically coherent rather than purely mathematical partitioning. However, solutions with more than 5 clusters increasingly produced diffuse memberships, fragmented temporal patterns, and reduced interpretability of both spectral and centroid structures. This progressive over-fragmentation was also evident in lower FPC values and high partition entropy at higher cluster dimensionalities (Fig.S3). Based on the combined evaluation of clustering stability, temporal coherence, spectral interpretability, and biologically meaningful stress separation, a five-cluster solution (c = 5) with a fuzziness coefficient of m = 1.6 was selected for downstream interpretation (Fig. 2).

In chestnut emissions, the cluster-1 centroid (C1; pre-stress cluster) dominated the pre-stress period and exhibited a pronounced diel cycle (Fig.2e), representing the primary constitutive emission before stress (Fig.2a,e). UWFCM additionally resolved a generalized stress cluster (C3) whose temporal dynamics were partially similar to those of the pre-stress cluster (cosine similarity index 0.46, Fig. S8). Despite this similarity in diel behavior, C3 showed a distinct spectral composition, including stress-associated compounds such as $C_{10}H_{15}^+$ (m/z 135.11), $C_9H_{15}^+$ (m/z 123.116), and phenol ($C_6H_7O^+$, m/z 95.05). A heat-stress cluster (C4) emerged during the heat-stress window, with strong diel behavior and a unique fingerprint spectrum. The significant transition observed during the combined heat and ozone stress window formed a distinct cluster characterized by strong diel behavior and minimal overlap with the pre-stress cluster (Fig. 2e).

A similar progression was observed in linden emissions, although the resolved clusters differed from those identified in chestnut emissions (Fig. 2 b, f). Distinct pre-stress (C1), heat-stress (C2), general stress cluster (C3) and extreme-heat (C5) clusters were resolved, with reflection of successive changes in mass spectral composition. The heat-stress cluster (C2) shared some temporal and spectral characteristics with the pre-stress cluster but became increasingly prominent following the pre-stress period and was accompanied by higher diel emission intensity, consistent with the heat-associated VOC signature. Unlike chestnut, no separate factor corresponding specifically to the combined heat and ozone treatment was identified. Instead, the heat-associated cluster persisted throughout the combined-stress period.

Cluster-2 in chestnut and Cluster-4 in linden showed fewer prominent temporal structures with low centroid and diffuse spectral profiles. To further investigate these clusters, diel emission patterns (Fig. 2 e, f) were evaluated to determine whether they were driven by biogenic emissions. Based on three lines of evidence, these clusters were interpreted as background-related rather than biological stress-driven.

Factor resolved stress-specific VOC fingerprints and biochemical pathways

The 5-cluster solution identified distinct stress-temporal VOC fingerprints across both chestnut and linden emissions, while simultaneously re-constructing biologically meaningful emission patterns (Fig. 3a-b). In chestnut emissions, the pre-stress emissions profile was dominated by $C_6H_7O^+$ (phenol), $C_8H_{11}^+$ (m/z 107.855) (Fig.3a), as consecutive physiological activity rather than stress-induced Lipoxygenase pathway (LOX) or terpenoids response. Pathway analysis associated this cluster mainly with the shikimate pathway (SKP) (Fig.3c), a major route of plant carbon metabolism through which up to ~30% of photosynthetically fixed carbon[67] can be directed to aromatic amino acids, benzenoids, phenylpropanoids, and related secondary metabolites. Previous studies have shown that plant VOC emissions can occur constitutively and that baseline VOC blends are species- and genotype-dependent chemotypic traits[45]. The background cluster 2 isolated weak, spectrally diffuse low-intensity signals with minimal temporal variation (Fig. 2 e), including intermittent masses with high uncertainty, effectively filtering out noisy VOCs. As stress developed, general stress fingerprint spectra (C3) shifted into a shared

pathway, SKP to LOX and MEP (Methylerythritol 4-Phosphate pathway) (Fig.3c), with increased oxygenated compounds, including $C_6H_7O_2^+$ (m/z 111.044), and $C_9H_{11}^+$ (m/z 119.085, a potential aromatic fragment or indane) (Table S2). This pattern is consistent with the literature, abiotic stress commonly induces oxygenated VOCs, arising from membrane lipid oxidation and stress-related cellular damage[68]. The pathway shifted from the baseline SKP metabolic pathway towards the LOX and methylerythritol phosphate (MEP) pathways under heat stress (C4) with a fingerprint signature of sesquiterpenes ($C_{15}H_{25}^+$, m/z 205.195), C5 carbonyls ($C_5H_9O^+$, m/z 85.0648), and monoterpenes ($C_{10}H_{17}^+$, m/z 137.132). The combined heat and ozone stress cluster (C5) was dominated by monoterpenes, $C_4H_7O^+$ (m/z 71.05, potentially MVK, MACR), and diterpenes ($C_{20}H_{33}^+$, m/z 273.25) (Table S2), which activate a stress-sensitive pathway called the methylerythritol phosphate (MEP) pathway. This is consistent with established terpenoid biosynthesis, where the cytosolic mevalonate (MVA) pathway primarily supplies precursors for sesquiterpenes, whereas the plastidial MEP pathway supplies precursors for hemiterpenes, monoterpenes and diterpenes[69].

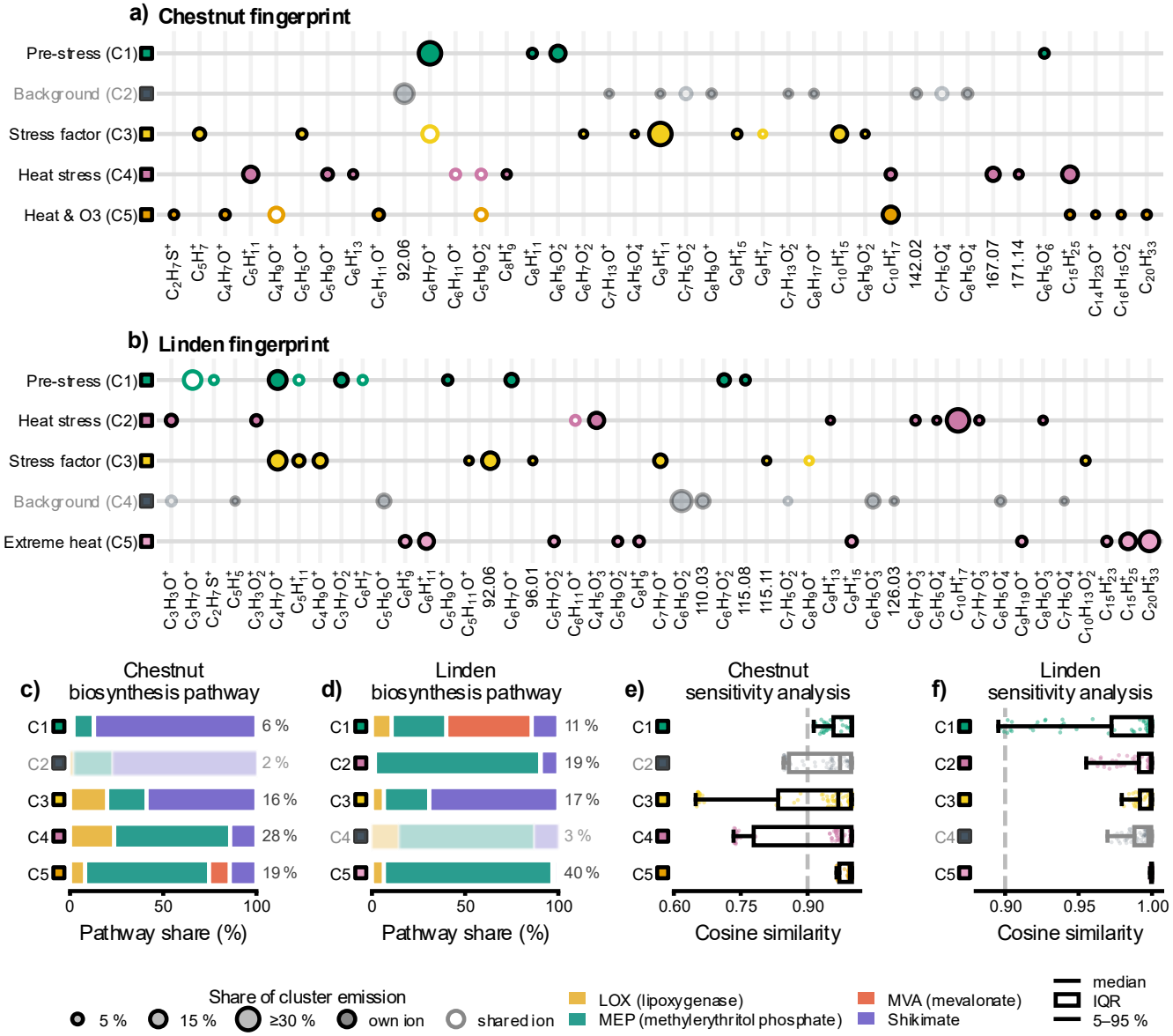


Figure 3 Cluster-resolved stress-associated BVOC emission fingerprints and their biosynthetic pathway contributions for chestnut and linden. (a,b) Uncertainty-weighted fuzzy c-means emission fingerprints for chestnut and linden, respectively. Circles represent individual VOC ions assigned to each cluster, with circle size proportional to their relative contribution to cluster emissions. (c,d) Relative contributions of four putative biosynthetic pathways to each cluster's emissions, attributed

by typical pathway tracers. Percentages at the end of each bar indicate the cluster's share of total emissions. Subplots (e–f) present Monte Carlo cluster stability based on cosine similarity between perturbed and baseline centroids after Hungarian matching. Colored dots represent individual Monte Carlo perturbation runs. Horizontal black lines indicate the cluster median similarity, vertical black bars represent the interquartile range (25th-75th percentile), and the lower and upper horizontal whiskers denote the 5th and 95th percentile similarity bounds, respectively.

A similar pre-stress metabolic transition was observed for linden, although the chemical fingerprints differed from those of chestnut (Fig.3b) and were primarily dominated by constitutive oxygenated and aromatic emissions (Fig. 2 d), including phenol, $C_5H_{11}^+$ (m/z 71.08, likely a pentanol fragment) and benzene (m/z 79.054) (Table S3). The heat-stress cluster was driven by monoterpene and $C_6H_{11}O^+$ (m/z 99.08, likely a green leaf volatile, hexenal), with MEP pathway activation (Fig.3d). The general stress factor was shaped by well-known stress-marker compounds hexenal, $C_4H_9O^+$ (C4 carbonyls, m/z 73.06), $C_5H_{11}^+$ (pentanol fragment) and $C_5H_{11}O^+$ (m/z 87.08, C5 carbonyls), whereas Cluster 4 isolated background-associated noise. Under the most severe thermal stress (cluster 5), the fingerprint shifted toward aromatic monoterpenes, sesquiterpenes, and diterpenes, resulting in the strongest contribution from the MEP-derived terpenoid synthesis pathway.

In linden emissions, there was significant overlap between heat and combined stress clusters, especially in oxygenated and alcohol-dominated emissions (Fig.S8). This explains why an independent combined heat and ozone stress factor, like cluster-5 in chestnut, was not identified. Cluster stability was further evaluated using a Monte Carlo sensitivity analysis (Fig.3e-f) (details in methods), in which cluster correspondence between perturbed and reference clusters was first resolved using the Hungarian assignment prior to the similarity comparison. Cosine similarity indices remained consistently high across perturbed cluster solutions, and the resolved stress-associated spectral fingerprints were reproducible against stochastic perturbations and uncertainty propagation.

Stress modifies the temperature-dependent coefficient

The UWFCM clustering of stress signature spectra raises the question of whether the major stress-associated fingerprint compounds, especially terpenoids, follow typical or altered temperature sensitivities. Global BVOC emission models, including MEGAN, are based on empirical temperature-response algorithms. It is therefore important to investigate how stress modified the exponential temperature-emission relationships, especially as recent syntheses suggest that temperature sensitivity (for monoterpenes and sesquiterpenes) is not static but dynamically reshaped by ecosystem stress and plant functional type[48,49]. Following the MEGAN framework[46], exponential fits were used to compare temperature sensitivities (β) across stress, although deviations from exponential behaviour indicate that temperature alone cannot explain all emission responses (Fig S9-S10).

Under pre-stress conditions, monoterpene emissions from linden closely matched the classical MEGAN parameterization (β ~0.10 °C^{-1}) (Fig. 4 for linden, Fig. S12 for both). They displayed strong exponential temperature-emission relationships (R^2=0.81) (Fig.S9), showing that monoterpene emissions were largely temperature-driven, described by the standard emission parameterization used in MEGAN[46,47]. Heat stress further increased monoterpenes temperature sensitivity, (β = 0.13 °C^{-1}; R^2 = 0.90, Fig.4a). This is consistent with recent evidence that the temperature sensitivity coefficient is not static[48], but can vary with species[70] (Fig., S11, S12), vegetation type, and other drivers[71,72], including heat stress. Under combined ozone-heat stress, the temperature sensitivity coefficient (β) for monoterpenes declined below the commonly used MEGAN 2.1 range (β = 0.09 °C^{-1}), with low R^2. Monoterpene emissions were thus no longer solely driven by temperature under oxidative stress.

A similar stress-dependent pattern was observed for diterpenes, but with substantially larger β-values. During heat stress, diterpene β-values reached approximately 0.20 °C^{-1} (Fig. 4c; Fig. S11c, S12c), a stronger temperature sensitivity than for monoterpenes under acute warming. An exponential temperature-response function was fitted to estimate and compare emission temperature sensitivities across stressors. Although some compounds (Fig.S9-S10) showed strong temperature dependence, others deviated from the exponential relationship, particularly under stress conditions, which also indicates that temperature alone did not fully explain the observed emission variability.

Sesquiterpene emissions showed relatively high temperature sensitivity under pre-stress (i.e. without any experimentally added stressor), with β-values close to or above the typical MEGAN temperature coefficient for sesquiterpenes (Fig.S11b,S12b,Fig.4b). These indicate that before stress exposure, sesquiterpene emissions were strongly temperature-responsive and broadly consistent with temperature-based emission parameterizations. However, as stress progressed, sesquiterpene temperature sensitivity declined, particularly under combined O_3 + heat stress, where β decreased to approximately 0.08 $°C^{-1}$. Although the corresponding R^2 values remained variable and in some cases relatively high (R^2 =0.65-0.93), the lower β-values show that the magnitude of the temperature response was substantially reduced under combined stress. Reduced β-values have been reported during periods when temperature alone does not dominate emission dynamics such as spring recovery or needle expansion in Norway spruce[14]. In addition, speciated SQT composition can shift over time, meaning that bulk SQT emissions may reflect changing mixtures of compounds with different temperature responses rather than a single uniform emission process[73,74].

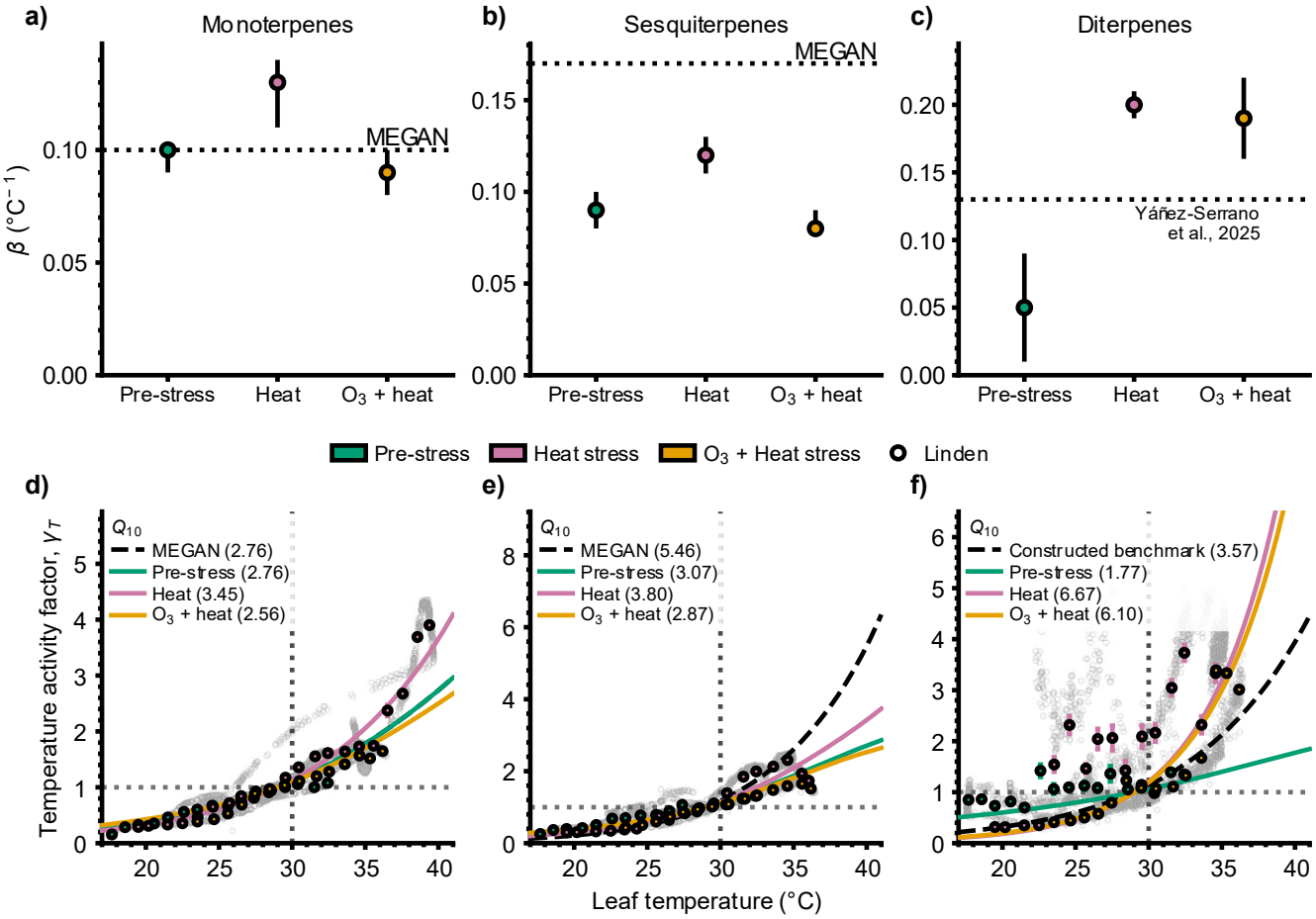


Figure 4 Stress-dependent temperature responses of terpenoid emissions of linden. (a–c) Temperature sensitivity coefficients (β) for monoterpenes, sesquiterpenes and diterpenes, respectively, under pre-stress, heat stress and combined ozone-heat stress conditions in linden. Points represent recommended β values from β exponential fits, and error bars represent the supported β range within 5% of the minimum RMSE. (d–f) Corresponding temperature activity factors (γ_t) as a function of leaf temperature. Grey circles represent individual normalized emission measurements from both species, and coloured squares indicate 1 °C temperature-bin means ± standard error. Solid curves show stress-specific temperature-response functions derived from MEGAN-based parameterizations, while dashed black curves indicate the reference MEGAN functions or, for diterpenes, a constructed benchmark. Q10 (dimensionless) is the multiplicative change in emission rate per 10 K. Vertical and horizontal dotted lines mark the reference temperature (30 °C) and normalized activity factor (γ_t = 1), respectively. Similar results are shown for chestnut in Fig. S11.

The results shown here for linden are similarly reproduced by the chestnut experiments (Fig S11). However, due to an issue in the experimental setup during the chestnut experiments (the inlet sampled not directly from the chamber, but from a reservoir connected to the chamber, see methods), the absolute β values are more uncertain for the chestnut emissions.

Together, these results highlight a major model uncertainty when using fixed β-values to represent stress-related terpenoids emissions. Our findings show that temperature-dependent terpene emission models should not rely only on fixed or plant-functional-type-based β-values. Although plant functional type dependent parameterizations are an improvement over universal coefficients, they may still be insufficient when emissions are affected by simultaneous heat and O_3 stress, because stress can alter the magnitude and even the direction of temperature sensitivity within the same vegetation type. Incorporating stress-dependent, and compound-class-specific β-values would therefore reduce uncertainty in isoprenoids emission estimates, especially under future atmospheric conditions where heat waves and elevated O_3 are likely to occur together.

Warming amplification

We calculated the Q_{10} coefficient from the fitted temperature-response curves between 20 and 30 °C (Fig.4d-f, Fig.S11, S12). Q10 (dimensionless) is the multiplicative change in emission rate per 10K. Without added stress and in the MEGAN parameterization, monoterpene emissions increased 2.7-fold under a 10°C leaf temperature increase (Fig. 4d). Heat stress increased this factor to ~4-fold, while combined heat+O3 stress reduced it to ~2-fold (Fig.S11-12). A global synthesis indicates that monoterpene emissions are more temperature-sensitive[48] than commonly represented in default model parameterizations[46], meaning that the stress-related case may be the scenario more common in nature.

For sesquiterpenes, the MEGAN reference has a $Q_{10}$of 5.46, whereas our experiments showed pre-stress, heat-stress and heat+O_3 Q_{10}values of ~4, ~3.6 and ~2.8, respectively (Fig.S12), i.e. a lower temperature sensitivity than MEGAN. The default model response overestimated sesquiterpene temperature sensitivity, which is congruent with the literature[49,75]. Diterpenes showed the strongest heat-induced temperature sensitivity increase and would increase normalized diterpene emissions by ~6-fold for a 10 °C rise. A strong temperature sensitivity remained even under combined heat and O_3 stress (Fig.4f, Fig.S12f). This is also consistent with recent ecosystem-scale observations from boreal wetlands[76], where diterpene fluxes showed strong temperature dependence with a Q_{10} value of 7.85.

Discussion and implications

UWFCM provides an uncertainty-aware framework for resolving stress-dependent VOC fingerprints from complex time-series emissions. UWFCM is complementary to classical source-apportionment methods such as PMF. While PMF is designed to resolve additive source-like factors, UWFCM is useful for identifying gradual and overlapping patterns in high-dimensional time-series data, particularly when measurement uncertainty and low-confidence signals need to be explicitly considered. By incorporating measurement uncertainty into noise-weighting functions, the model reduces the influence of weak, noisy, or inconsistently detected signals, allowing chemically coherent emission fingerprints to emerge.

However, UWFCM-derived fingerprints should not be interpreted blindly. As an unsupervised approach, the model identifies statistical structure in the data, but the chemical and biological meaning of each factor still requires expert evaluation. This is particularly important for PTR-ToF-MS data, where isomeric compounds, water clusters, and parent-ion fragmentation can complicate compound annotation. In addition, cluster solutions depend on preprocessing choices, uncertainty estimates and the selected number of clusters. Robustness should therefore be assessed through sensitivity tests, repeated initialization, independent compound validation or complementary physiological measurements. Because the model learns structure from the observed dataset, it may also require recalibration before being transferred to other species, stress combinations or field conditions.

Despite these limitations, UWFCM has broader value for atmospheric chemistry and ecosystem monitoring. Beyond controlled plant-chamber experiments, uncertainty-aware fuzzy clustering could be applied to forest flux-tower datasets,

urban vegetation monitoring, chemical ionization mass spectral field data, and early-warning detection of ecosystem stress. We showed that plant stress increases the amount of carbon emitted to the atmosphere. However, it can also alter the chemical composition of the emitted blend. Such shifts can change atmospheric chemistry and thereby influence secondary organic aerosol and ozone formation.

Our findings suggest that stress not only alters total BVOC release but also changes the degree to which reactive emissions scale with warming. Urban vegetation can contribute more than half of the organic reactivity during heat periods[77] and can directly enhance peak ozone formation[78]. Thus, stronger temperature-driven emissions from urban trees, as we observed, are expected to increase the precursor supply for ozone and SOA formation during heat events (Fig.5). If monoterpene, sesquiterpene, and diterpene emissions increase several-fold with warming, as in our study, the potential supply of precursors for SOA and ozone formation may increase by a similar factor, although the aerosol and ozone burden will depend on oxidant concentrations, NOx, particle sinks, and boundary-layer dynamics.

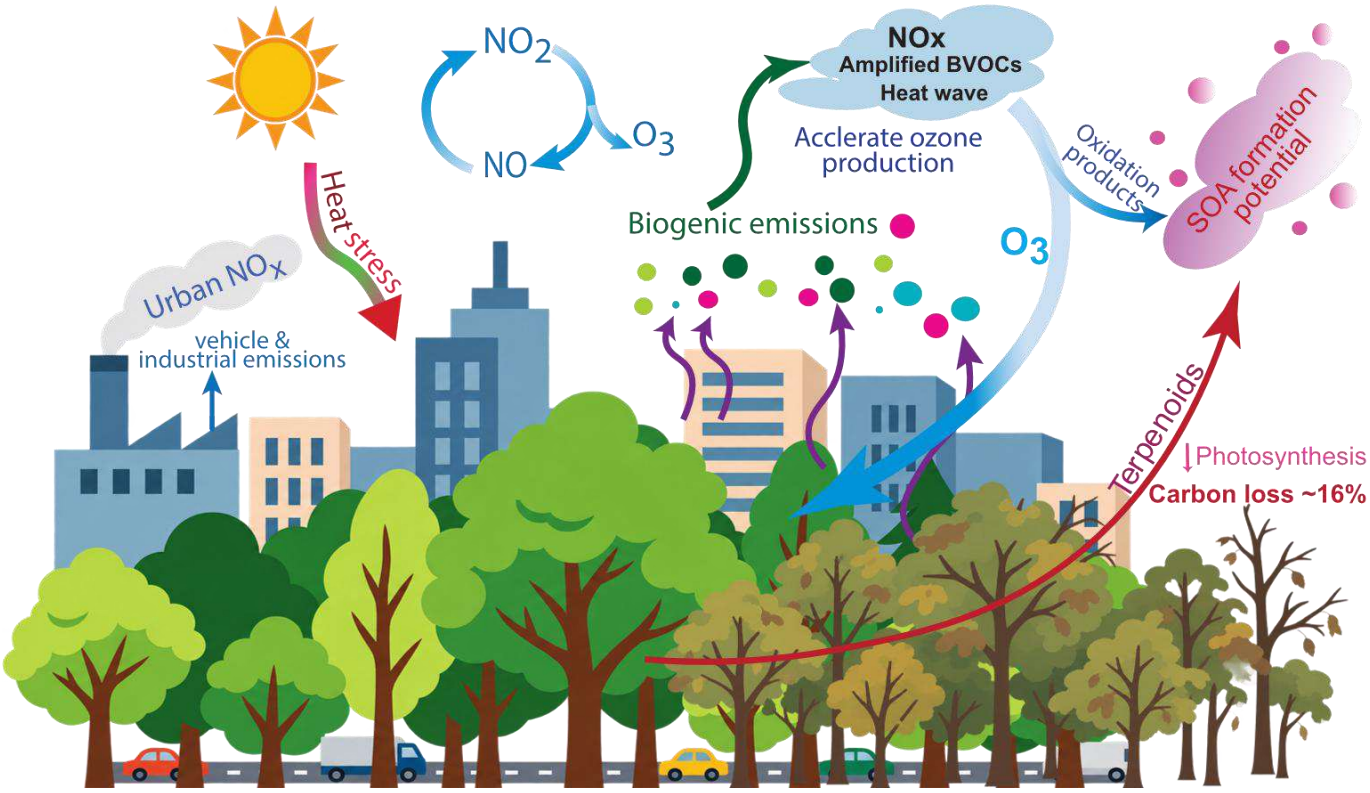


Figure 5 Conceptual framework of heat-BVOC-ozone interactions in an urban environment. Heat waves increase the overall BVOC emissions, which interact with urban NO_x and sunlight to increase ozone and SOA formation potential. The added stress from ozone and heat can reduce plant photosynthetic efficiency and increase daytime carbon loss rather than carbon uptake. (This content was designed with Adobe Illustrator by B.D.)

Methods

Chamber setup

Stress experiments were conducted in SAPHIR-PLUS (Plant Chamber Unit for Simulation) coupled with the atmosphere simulation chamber SAPHIR (Simulation of Atmospheric PHotochemistry In a large Reaction Chamber) at Forschungszentrum Jülich, Germany, during summer 2025. The PLUS chamber is a rectangular, airtight container with temperature and photosynthetic light controls, a double-walled 9.32 m³ Teflon film enclosure that can house up to six trees, with a maximum height of 1.5 meters[79]. To ensure homogeneous steady conditions within the PLUS enclosure, synthetic air

of 100 L/min was passed using turbulent airflow. The PLUS enclosure is isolated from the soil to ensure that air samples are collected specifically from the leaves.

Two tree species commonly planted in cities[50] were selected for the experiment: chestnut (*Castanea sativa*) and linden (*Tilia cordata*). 18 saplings (~1.3 m height) of chestnut (n=9) and linden (n = 9) were acquired from a local nursery and maintained outdoors for ~3.5 months after transplanting into fresh soil. Plants were regularly watered and screened for visible disease and pest damage. As the PLUS chamber accommodates a maximum of six trees, six individuals were used per experimental run. Six of the healthiest trees in terms of being free of disease and pests, and with straight stems, were selected for the experiment. After placing the plants into the chamber, the enclosure was kept slightly overpressurized to prevent trace gases from diffusing into the plant chamber. The pressure difference between the chamber wall and the Teflon enclosure (~3-8 Pa) was used to verify that there were no leaks from the soil or canopy parts. Constant light intensity of ~800 µmol m^{-2} s^{-1} and optimum soil moisture (55-80% volumetric water content, UMS GmbH München, EC-5 sensor) were maintained during daytime (06:00-18:00 UTC). 400 ppm CO_2 was mixed with the synthetic air to support the plant's photosynthesis. The leaf area was measured using a LI-COR Plant Canopy Analyzer following the isolated-tree measurement protocol. To minimize instrumental and operator bias, measurements were independently repeated three times, and the average was used for subsequent analyses.

Treatments were applied sequentially to the same six sets of individuals, with air sampled from the canopy. Following the pre-stress, heat (20 °C to 38 °C) and combined ozone-heat stress were periodically introduced (Fig. S13). Ozone fumigation lasted 48-72 hours at ~120 ppb, and after the fumigation, the enclosure was flushed to remove all ozone. Sequential stress was applied to simulate real-world scenarios where the same area experiences heatwaves and/or ozone pollution, either simultaneously or consecutively.

Temperature ramps were conducted to measure temperature-dependent emissions under each stress condition. During the night before each ramp experiment, chamber temperatures were set to ~18°C. The following day, temperatures were gradually increased in steps to ~40°C (Fig.S13).

Plant emission measurements

Canopy emissions from the PLUS enclosure were continuously sampled (3 L/min) through a heated and thermally insulated perfluoroalkoxy alkane (PFA) inlet line to minimize compound losses and condensation artifacts. Online measurements were performed using a fast GC-coupled proton-transfer-reaction time-of-flight mass spectrometer (FUSION PTR-TOF) operated in H_3O^+ reagent ion mode with a mass resolution of 10,000. During the measurement period, drift tube pressure was ~3.22 mbar, with a 358 V drift voltage. A fastGC measurement was performed once every hour on a non-polar column (MXT-5, Restek). Each GC run lasted 180 s and the temperature ramp was programmed from 40°C to 230°C with a plateau at 230°C for 16 s before the cooling down phase. The information from the fastGC was used to identify fragmentation and isomers in the PTR measurements. Ions affected by fragmentation or by several isomers were corrected using these GC-derived contributions. For example, *m/z* 69.070 ($C_5H_9^+$), commonly attributed to isoprene, contained ≤ 2% isoprene in most phases and was dominated by fragments of aldehydes (Fig.S2). Its signal was therefore reassigned to these compound classes rather than to isoprene, and the carbon number used in carbon-budget calculations was weighted by the GC-derived contributions. Where an ion comprised of several isomers, the name of the main contributing isomer is used in the text, and the full GC-resolved composition is given in Supplementary Fig. S2.

A certified standard gas mixture with 17 compounds (Apel-Riemer Inc., USA), ranging from mass-to-charge ratio m/z 33 to m/z 371, was used for daily calibration. Zero-air measurements were performed hourly for instrument background subtraction. Mass spectral peak identification and peak fitting were conducted using IONICON Data Analyzer (IDA) software based on exact mass and isotopic distribution. Canopy emission rates were estimated from background-corrected concentrations using the enclosure flow rate and the leaf area index according to Edtbauer et al.[80]. Relative uncertainties were propagated assuming independent error sources and combined in quadrature. For theoretically calibrated compounds, uncertainties associated with reaction-rate constants, flow control, calibration fitting, calibration standards and signal

variability resulted in an overall uncertainty of ~51%. The limits of detection for the compounds are listed in Table S4 of the supplementary information.

During the chestnut experiment, the FUSION PTR-ToF-MS inlet inadvertently sampled air from an interspace behind the PLUS chamber inlet because the inlet had been accidentally pulled out of its original position. This caused sampling of the chamber air via a reservoir between the outer and inner Teflon walls of the chamber, potentially dampening VOC emission profiles (more in Supplementary Information Section 04). The FUSION inlet was repositioned on 30 July 2025, before the linden heat stress measurements, which were therefore unaffected by this inlet-positioning issue. Relative changes are the main focus of this manuscript and are not affected. Potential inlet-related biases in chestnut measurements are likely a reduction in absolute observed emissions and a dampened diel cycle. None of this affects the reported relative changes or the UWFMC fingerprinting model.

Relative carbon re-emission through VOCs

Relative carbon loss through VOC emissions was quantified from the BVOC emission rates with net daytime CO_2 uptake ($|CO_2|$). Total carbon-equivalent BVOC fluxes for each compound were estimated by equation (1), where E_i is the emission rate of the compound i ($nmol.m^{-2}.s^{-1}$) and $n_{C,i}$ is the corresponding carbon number of compound i. The ratio between the carbon fixation and VOC-derived carbon loss relative to VOC carbon loss was then calculated using equation 2.

$$C_{VOC} = \sum_{i=1}^{n} (E_i \times n_{C,i}) \quad (1)$$

$$\text{Relative VOC carbon loss (\%)} = \frac{C_{VOC}}{|CO_2|} \times 100 \quad (2)$$

Uncertainty Weighted Fuzzy C-means Clustering

Source apportionment has traditionally relied on either supervised machine-learning approaches or unsupervised factorization techniques, such as positive matrix factorisation (PMF). Supervised learning models, including random forests and neural networks, are highly effective for distinguishing known training information and require labelled training data; these approaches cannot directly discover previously unknown physiological states, transitional responses, or mixed stress signatures.

Although both positive matrix factorization (PMF) and uncertainty-weighted fuzzy c-means (UWFCM) are unsupervised approaches, they address fundamentally different analytical objectives. PMF is a matrix-factorization technique that decomposes the observation matrix into latent factor profiles and their temporal contributions. The method seeks the factor combination that best reconstructs the measured data while minimizing uncertainty-weighted residuals. Consequently, PMF is particularly suited for resolving underlying emission sources that contribute to the observed signal. In contrast, UWFCM is a similarity-based clustering framework that does not attempt to reconstruct the observation matrix. Instead, it groups time traces (here: VOCs) based on similarities in their temporal behaviour and assigns fuzzy memberships that allow compounds to partially belong to multiple clusters. This is particularly relevant for plant or ecosystem stress responses, where VOC emissions frequently arise from overlapping biochemical pathways and gradual temporal or physiological transitions rather than discrete additive sources. Both analytical approaches are complementary rather than competing.

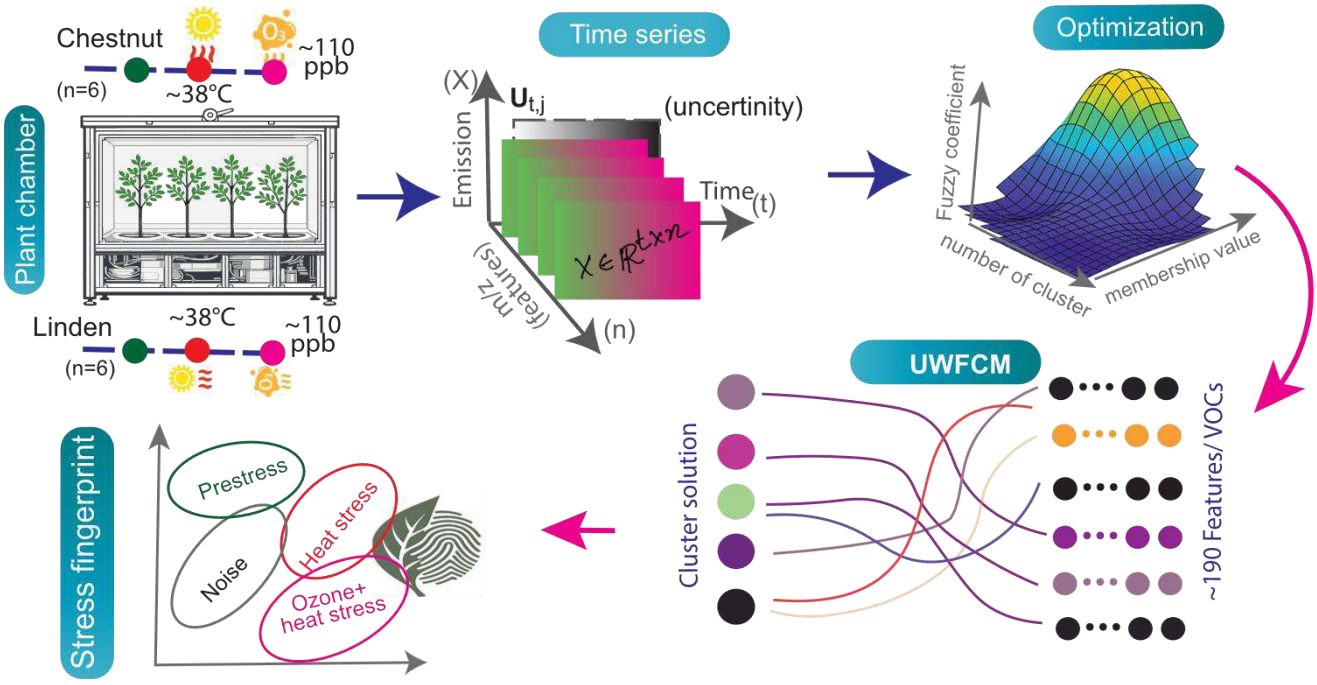


Figure 6 Conceptual methodological framework. Chestnut and Linden trees were subjected to sequential heat and combined ozone–heat stresses in controlled plant chambers. Plant emissions were continuously measured using PTR-ToF-MS. After preprocessing, high-dimensional time series and uncertainty matrix were used to identify the stress fingerprint using an uncertainty-weighted fuzzy clustering algorithm.

Uncertainty estimation

The emission rate for linden and chestnut was set as a data matrix $X_{\text{emission rate}} \in \mathbb{R}^{t \times n}$, where t is the time points, and n represents the number of VOCs (as a feature) (Fig.6). Measurement uncertainty (uncertainty matrix, $U_{t,j}$) for each VOC j at time t was quantified using a quadratic error equation (Eq.3). This combines a signal-dependent component with a detection-limit-based component to account for precision and accuracy. For signals above the detection limit $X_{t,j}$ (measured emission rate of compound j at time t) > $\text{LOD}_{t,j}$ (limit of detection), and signals at or below the detection limit ($X_{t,j} \leq \text{LOD}_{t,j}$). Detection limits were computed as three standard deviations of the interpolated instrument background. The relative error fraction (EF) is the instrument's relative precision, estimated for each compound .

$$u_{t,j} = \sqrt{\left(EF_j \cdot |X_{t,j}|\right)^2 + \left(\frac{\text{LOD}_{t,j}}{3}\right)^2} \qquad (3)$$

To quantify the compound-specific signal reliability, two metrics, detection reliability (f_j) and signal-to-uncertainty ratio (SUR) were derived from the uncertainty matrix. Where T is the total number of observations and $I(\cdot)$ is the indicator function, which equals 1 when the condition is satisfied and 0 otherwise.

$$f_j = \frac{1}{T} \sum_{t=1}^{T} I(X_{t,j} > \text{LOD}_{t,j}) \quad (4)$$

$$\text{SUR}_j = \text{median}_t \left(\frac{|X_{t,j}|}{U_{t,j}}\right) \quad (5)$$

Uncertainty-weighted fuzzy c-means clustering

Clustering was analyzed using an uncertainty-weighted fuzzy C-means (UWFCM) algorithm to identify temporally coherent emission patterns, which were subsequently interpreted to derive stress-associated VOC fingerprints. The data matrix was structured so that each VOC represented an individual sample characterized by its temporal emission profile throughout the

experimental period. Therefore, clustering was performed on VOC features rather than time points, to group VOC compounds with similar temporal dynamics and stress-response behavior. Each VOC was normalized (L2 (Euclidean) normalization, min-max, and z-score normalization) using row-wise transformation for reducing the emission magnitude effects and emphasizing the relative temporal structure. Uncertainty enters per measurement rather than per compound, each squared residual being weighted by the inverse variance of the cell. This retains the time dimension of uncertainty, which distinguishes a compound that is noisy throughout from one that is noisy only while its emission is low.

Uncertainty enters the algorithm at a single point. Each squared residual between a transformed profile and a cluster centroid is weighted by the inverse variance of that cell, so that better-measured observations constrain the solution more strongly than poorly measured ones. Here x′(t,j) denotes the transformed, uncertainty-propagated profile of VOC j at time t, and the cluster centroids v(k,t) were estimated using Eq.6, in which u(k,j) is the membership of VOC j in cluster k and m is the fuzzifier controlling the degree of cluster overlap. The clustering objective was modified accordingly using Eq.7, with the per-cell weight defined in Eq.8. A centroid is therefore itself a time series and can be read directly as the temporal pattern defining its cluster. To ensure robustness against local minima the clustering was repeated from independent random initialisations and the best-scoring solution retained; for each run, partition certainty was evaluated by the fuzzy partition coefficient (FPC) Eq.9. and the partition entropy (PE) Eq.10, which are reported as descriptive diagnostics rather than as selection criteria.

$$v_k = \frac{\sum_{j=1}^{N} u_{k,j}^{m} w_j x'_j}{\sum_{j=1}^{N} u_{k,j}^{m} w_j} \quad (6)$$

$$Jm = \sum_{k=1}^{c} \sum_{j=1}^{n} w_j \; u_{kj}^{m} \; \| \; x'_j - v_k \; \|^2 \quad (7)$$

$$W_{t,j} = \frac{1}{(u'_{t,j})^2}, \; W_{t,j} = 0 \;\; \text{for an unmeasured cell} \quad (8)$$

$$FPC = \frac{1}{n} \sum_{k=1}^{c} \sum_{j=1}^{n} u_{kj}^2 \quad (9)$$

$$PE = -\frac{1}{n} \sum_{k=1}^{c} \sum_{j=1}^{n} u_{k,j} \log(u_{k,j}) \quad (10)$$

Where c and n are the number of clusters and the number of VOCs respectively, T is the number of time points, and t indexes time; $u_{k,j}$ represents the fuzzy membership of VOC j in cluster k; v_k denotes the centroid of cluster k at time t; w_j is the per-cell inverse-variance weight defined in equation 12a, and m is the fuzzifier controlling cluster overlap.

The relative importance of each VOCs within a cluster was subsequently measured using a weighted membership score, $score_{k,j} = u_{k,j}^{m} \cdot w_j$, which shows both cluster association strength and the underlying signal reliability. For interpretation, cluster-specific spectra were reconstructed as $S_k(j) = u_{k,j} \cdot w_j \cdot b_j$, where $b_j$refers to the global median emission of VOC j. Candidate solutions were compared using multiple complementary clustering indices across these metrics, the silhouette score, the Davies–Bouldin index, the Calinski–Harabasz index, the Xie–Beni index, including FPC, and PE. Details of these indices are provided in Wu et al[44]. The final cluster solution was selected based on combined diagnostic evidence (statistical and biological) rather than a single metric. It was also evaluated based on biological interpretability, including the coherence of spectral profiles, dominant VOC contributions, and distinct diel temporal patterns of the resolved factors. Although the original emissions were measured in nmol m^{-2} s^{-1}, clustering was performed on transformed (L2-normalized) and uncertainty-weighted profiles. Consequently, cluster centroids and cluster intensity are reported as normalized unitless

quantities. Cluster contribution spectra represent relative VOC importance within each cluster and should therefore be interpreted comparatively rather than as direct emission rates.

Sensitivity analysis

A Monte Carlo–based sensitivity analysis was evaluated to assess the robustness, elasticity and reproducibility of UFCM solutions for chestnut and linden. The reference cluster was the resolved 5-cluster solution, which was used as the baseline reference spectra for all subsequent comparisons. UFCM sensitivity was assessed repeatedly by perturbing different matrices and rerunning the full UFCM workflow. For robustness in terms of measurement, instrumental variability, five perturbation sources were used, (i) different seed initialization; (ii) adding Gaussian noise to the emission or data matrix; (iii) randomized features or compounds (m/z) dropout; (iv) time-block dropout; and (v) changing the uncertainty-weighting or tuning parameters.

Gaussian perturbations were applied to each VOC time series at four relative scales: 0, 0.05, 0.10, and 0.20. These perturbations were scaled by the standard deviation of each compound time series, so that those with higher variance received proportionally larger perturbations than those with lower variance, thereby simulating realistic, magnitude-dependent uncertainty. Features (VOCs) were randomly removed (0.5%, and 10%) to assess dependence on individual compounds. For contiguous time-block dropout, a continuous segment of the VOC time series was randomly removed or masked before rerunning the UFCM. Unlike random point-wise removal, this approach conserves the realistic temporal structure of missing observations. Weight sensitivity was evaluated by changing the parameters ($w_{\min}, S_t, \gamma_{low}\ and\ \gamma_{high}$) that controls the uncertainty-to-weight transformation. Three sets of weighting representing baseline, mild, and strong noise penalization were evaluated, baseline ($w_{\min} = 0.001$, $S_t = 0.5$, $\gamma_{low} = 2$, $\gamma_{high} = 8$), mild (0.01,0.6,1.5,5), and strong (0.0005,0.4,3,10).

Cluster identities or numbers in unsupervised clustering are arbitrary and may change between runs; therefore, direct label-wise comparison between reference and perturbed clustering solutions is not rational. Therefore, correspondence between reference and perturbed centroids was resolved using the Hungarian assignment algorithm. This Hungarian algorithm identifies the globally optimal one-to-one cluster matching by minimizing centroid dissimilarity. Following cluster alignment, cosine similarity (Cos_{sim}) were used between matched baseline ($\overrightarrow{C_{ref}}$) and perturbed cluster ($\overrightarrow{C_{pt}}$) centroids.

$$Cos_{sim}(C_{ref}, C_{pt}) = \frac{\overrightarrow{C_{ref}} . \overrightarrow{C_{pt}}}{\|\overrightarrow{C_{ref}}\| \|\overrightarrow{C_{pt}}\|} \quad (11)$$

Temperature-dependent emission activity

The temperature sensitivity of major stress-fingerprint VOC classes was estimated to evaluate how stress modifies the thermal amplification of emissions under stress. Emissions were normalized separately for each tree species, compound, and stress type by dividing each emission rate by the median emission rate measured at leaf temperatures of 28-30 °C. Normalized temperature activity factors were then combined across chestnut and linden to be compared independently of species-specific differences stress-specific temperature responses. For isoprene, the G99[81] equation (12) was used directly because isoprene emissions treated as a predominantly light-dependent[46]. where $R = 0.00831$ kJ K^{-1} mol^{-1}, T is the leaf temperature in K, E_{opt} is the emission activity at the optimum temperature, C_{T1} and C_{T2} are empirical temperature-response parameters, and T_{opt} is the optimum temperature. A detailed comparison of air and leaf temperature sensors and an analysis of sensor robustness are in Fig. S14. The default isoprene parameters were $E_{opt} = 2.0$, $C_{T1} = 95$ kJ mol^{-1}, $C_{T2} = 230$ kJ mol^{-1}, and $T_{opt} = 313$ K (40 °C).

$$\gamma_{T,G99} = E_{opt} \frac{C_{T2}\exp(C_{T1}x)}{C_{T2} - C_{T1}[1-\exp(C_{T2}x)]} \text{ with } x = \frac{(1/T_{opt}) - (1/T)}{R} \quad (12)$$

Monoterpene, sesquiterpene, and diterpene temperature responses are represented as a combination of light-independent and light-dependent fractions and can be describe as Eq.13. LDF is the light-dependent fraction and $\gamma_{T,LIF}$, light-

independent component estimated using Eq.14. Where $T_s = 297$ K, the MEGAN2.1 standard reference temperature. This MEGAN2.1 standard temperature is distinct from the observational normalization temperature used for the plotted γT values.

$$\gamma_T = (1 - LDF)\gamma_{T,LIF} + LDF\gamma_{T,G99} \quad (13)$$

$$\gamma_{T,LIF} = \exp[\beta(T - T_s)] \quad (14)$$

For monoterpenes and sesquiterpenes parametrization, MEGAN2.1 values were used as reference[46], with $\beta = 0.10\ K^{-1}$, $LDF = 0.40$, $C_{T1} = 80$ kJ mol^{-1}, and $E_{opt} = 1.83$ for monoterpenes, and $\beta = 0.17\ K^{-1}$, $LDF = 0.50$, $C_{T1} = 130$ kJ mol^{-1}, and $E_{opt} = 2.37$ for sesquiterpenes. β-Pinene was used as a surrogate for diterpenes because both β-pinene and kaurene contain an exocyclic double bond, and diterpene parameters were unavailable in MEGANv2.04; we therefore applied $LDF = 0.20$, $C_{T1} = 80$ kJ mol^{-1}, and $E_{opt} = 1.83$. A β coefficient of 0.13 K^{-1} used as reported by recent literature[82]. To estimate how strongly emissions will respond to warming, Q_{10}values were calculated from the fitted temperature-response curves using Eq. (15). Q_{10}represents the fold change in normalized emission activity over a 10 K temperature increase.

$$Q_{10} = \left[\frac{\gamma_T(T_2)}{\gamma_T(T_1)}\right]^{\frac{10}{T_2 - T_1}} \quad (15)$$

Data and code availability

The datasets used for the study are available in publicly accessible repositories Dey et al., 2026[83]. The UWFCM software developed in this study is publicly available at https://github.com/biplobforestry/Uncertainty-Weighted-Fuzzy-C-means-Clustering . The framework integrates measurement uncertainty directly into fuzzy clustering to identify hidden patterns in complex datasets. Although developed for VOC stress-fingerprint analysis, it is transferable to source apportionment, atmospheric chemistry, environmental sensing, ecological monitoring, and other high-dimensional time-series applications.

Acknowledgments

The authors gratefully acknowledge Özgür Erdogan, Sergej Wedel, Niklas Ruland and Achim Grasse for their valuable technical support and assistance during the experiment and chamber operation.

Author contributions

E.Y.P., A.N. and T.H. conceptualized the study. B.D. performed the data analysis, visualizations and wrote the original manuscript draft. C.D. analysed the gas chromatography data. T.H., A.N, E.P, and H.F were responsible for the SAPHIR-PLUS chamber system and its operation. E.Y.P. performed data calibration and validated the analyses, secured funding and supervised the study. All authors participated in the experimental campaign, contributed to reviewing and editing the manuscript, and approved the final version.

Financial support

This work was supported by the Helmholtz Struktur- und Investmentfonds through a Helmholtz Investigator Group (grant no. VH-NG-20-17).

Competing interests

The authors declare no competing interests.

Clinical trial

Not applicable

Consent to participate declaration

Not applicable

References

(1) Knutzen, F.; Averbeck, P.; Barrasso, C.; Bouwer, L. M.; Gardiner, B.; Grünzweig, J. M.; Hänel, S.; Haustein, K.; Johannessen, M. R.; Kollet, S.; Müller, M. M.; Pietikäinen, J. P.; Pietras-Couffignal, K.; Pinto, J. G.; Rechid, D.; Rousi, E.; Russo, A.; Suarez-Gutierrez, L.; Veit, S.; Wendler, J.; Xoplaki, E.; Gliksman, D. Impacts on and Damage to European Forests from the 2018-2022 Heat and Drought Events. Natural Hazards and Earth System Sciences **2025**, 25 (1), 77–117. https://doi.org/10.5194/NHESS-25-77-2025.

(2) Fischer, E. M.; Sippel, S.; Knutti, R. Increasing Probability of Record-Shattering Climate Extremes. Nature Climate Change 2021 11:8 **2021**, 11 (8), 689–695. https://doi.org/10.1038/s41558-021-01092-9.

(3) Perkins-Kirkpatrick, S. E.; Lewis, S. C. Increasing Trends in Regional Heatwaves. Nature Communications 2020 11:1 **2020**, 11 (1), 3357-. https://doi.org/10.1038/s41467-020-16970-7.

(4) Grünig, M.; Rammer, W.; Senf, C.; Albrich, K.; André, F.; Augustynczik, A. L. D.; Baumann, M.; Bohn, F. J.; Bouwman, M.; Bugmann, H.; Collalti, A.; Cristal, I.; Dalmonech, D.; Coligny, F. De; Dobor, L.; Dollinger, C.; Espelta, J. M.; Forrester, D. I.; Garcia-Gonzalo, J.; González-Olabarria, J. R.; Hiltner, U.; Hlásny, T.; Honkaniemi, J.; Huber, N.; Jonard, M.; Jönsson, A. M.; Kunstler, G.; Lagergren, F.; Lindner, M.; Mina, M.; Moos, C.; Morin, X.; Muys, B.; Nabuurs, G.-J.; Nieberg, M.; Patacca, M.; Peltoniemi, M.; Reyer, C. P. O.; Schelhaas, M.-J.; Storms, I.; Thom, D.; Toïgo, M.; Seidl, R. Climate Change Will Increase Forest Disturbances in Europe throughout the 21st Century. Science **2026**, 391 (6789). https://doi.org/10.1126/SCIENCE.ADX6329.

(5) Wang, N.; Duan, F.; Shan, L.; Zhang, S.; Ma, Y.; Zhang, Q.; Zhu, L.; Wang, S.; Jiang, J.; Huang, T.; Kimoto, T.; He, K. Impacts of Intensified Heatwaves on Escalation of Ozone and Reactive Nitrogen in Summer. Environmental science & technology **2026**, 60 (1), 887–901. https://doi.org/10.1021/acs.est.5c09309.

(6) Wang, C.; Hu, X. M.; Feron, S.; Leffel, J.; Cordero, R. R. Compound Heat and Ozone Pollution in the Urban Environment. Urban Climate **2025**, 62 (June). https://doi.org/10.1016/j.uclim.2025.102511.

(7) He, C.; Lu, X.; Wang, H.; Wang, H.; Li, Y.; He, G.; He, Y.; Wang, Y.; Zhang, Y.; Liu, Y.; Fan, Q.; Fan, S. The Unexpected High Frequency of Nocturnal Surface Ozone Enhancement Events over China: Characteristics and Mechanisms. Atmospheric Chemistry and Physics **2022**, 22 (23), 15243–15261. https://doi.org/10.5194/ACP-22-15243-2022.

(8) Maison, A.; Lugon, L.; Park, S. J.; Baudic, A.; Cantrell, C.; Couvidat, F.; D'Anna, B.; Di Biagio, C.; Gratien, A.; Gros, V.; Kalalian, C.; Kammer, J.; Michoud, V.; Petit, J. E.; Shahin, M.; Simon, L.; Valari, M.; Vigneron, J.; Tuzet, A.; Sartelet, K. Significant Impact of Urban Tree Biogenic Emissions on Air Quality Estimated by a Bottom-up Inventory and Chemistry Transport Modeling. Atmospheric Chemistry and Physics **2024**, 24 (10), 6011–6046. https://doi.org/10.5194/ACP-24-6011-2024.

(9) Emmerichs, T.; Taraborrelli, D.; Shen, F.; Gromov, S.; Hegglin, M. I.; Wahner, A. Widespread Reduction of Ozone Extremes in Storylines of Future Climate. npj Clean Air 2025 **2025**, 1 (1), 19. https://doi.org/10.1038/s44407-025-00019-4.

(10) Ferretti, M.; Cools, N.; Dörner, M. L.; Michel, A.; Schwärzel, K.; Verstraeten, A.; Waldner, P.; Editors (2025). On the Pulse of Europeanforests. 40 Years of Pan-European Forest Monitoring: From Air Pollution to Climate Change. ICP Forests 40th Anniversary Report under the UNECE Convention on Long-range Transboundary Air Pollution (Air Convention). Eberswalde: Thünen Institute **2025**. https://doi.org/10.3220/253-2025-21.

(11) Brosset, A.; Blande, J. D. Volatile-Mediated Plant–Plant Interactions: Volatile Organic Compounds as Modulators

of Receiver Plant Defence, Growth, and Reproduction. Journal of Experimental Botany **2022**, 73 (2), 511–528. https://doi.org/10.1093/JXB/ERAB487.

(12) Rosenkranz, M.; Chen, Y.; Zhu, P.; Vlot, A. C. Volatile Terpenes – Mediators of Plant-to-Plant Communication. Plant Journal **2021**, 108 (3), 617–631. https://doi.org/10.1111/TPJ.15453.

(13) Sasaki, K.; Saito, T.; Lämsä, M.; Oksman-Caldentey, K. M.; Suzuki, M.; Ohyama, K.; Muranaka, T.; Ohara, K.; Yazaki, K. Plants Utilize Isoprene Emission as a Thermotolerance Mechanism. Plant and Cell Physiology **2007**, 48 (9), 1254–1262. https://doi.org/10.1093/PCP/PCM104.

(14) Bourtsoukidis, E.; Bonn, B.; Dittmann, A.; Hakola, H.; Hellén, H.; Jacobi, S. Ozone Stress as a Driving Force of Sesquiterpene Emissions: A Suggested Parameterisation. Biogeosciences **2012**, 9 (11), 4337–4352. https://doi.org/10.5194/BG-9-4337-2012.

(15) Singh, A. A.; Ghosh, A.; Agrawal, M.; Agrawal, S. B. Secondary Metabolites Responses of Plants Exposed to Ozone: An Update. Environmental Science and Pollution Research **2023**, 30 (38), 88281–88312. https://doi.org/10.1007/S11356-023-28634-2.

(16) Kesselmeier, J.; Ciccioli, P.; Kuhn, U.; Stefani, P.; Biesenthal, T.; Rottenberger, S.; Wolf, A.; Vitullo, M.; Valentini, R.; Nobre, A.; Kabat, P.; Andreae, M. O. Volatile Organic Compound Emissions in Relation to Plant Carbon Fixation and the Terrestrial Carbon Budget. Global Biogeochemical Cycles **2002**, 16 (4), 73–1. https://doi.org/10.1029/2001GB001813.

(17) Zhang, H.; Yee, L. D.; Lee, B. H.; Curtis, M. P.; Worton, D. R.; Isaacman-VanWertz, G.; Offenberg, J. H.; Lewandowski, M.; Kleindienst, T. E.; Beaver, M. R.; Holder, A. L.; Lonneman, W. A.; Docherty, K. S.; Jaoui, M.; Pye, H. O. T.; Hu, W.; Day, D. A.; Campuzano-Jost, P.; Jimenez, J. L.; Guo, H.; Weber, R. J.; De Gouw, J.; Koss, A. R.; Edgerton, E. S.; Brune, W.; Mohr, C.; Lopez-Hilfiker, F. D.; Lutz, A.; Kreisberg, N. M.; Spielman, S. R.; Hering, S. V.; Wilson, K. R.; Thornton, J. A.; Goldstein, A. H. Monoterpenes Are the Largest Source of Summertime Organic Aerosol in the Southeastern United States. Proceedings of the National Academy of Sciences of the United States of America **2018**, 115 (9), 2038–2043. https://doi.org/10.1073/PNAS.1717513115.

(18) Kavouras, I. G.; Mihalopoulos, N.; Stephanou, E. G. Formation of Atmospheric Particles from Organic Acids Produced by Forests. Nature 1998 395:6703 **1998**, 395 (6703), 683–686. https://doi.org/10.1038/27179.

(19) Birami, B.; Bamberger, I.; Ghirardo, A.; Grote, R.; Arneth, A.; Gaona-Colmán, E.; Nadal-Sala, D.; Ruehr, N. K. Heatwave Frequency and Seedling Death Alter Stress-Specific Emissions of Volatile Organic Compounds in Aleppo Pine. Oecologia 2021 197:4 **2021**, 197 (4), 939–956. https://doi.org/10.1007/S00442-021-04905-Y.

(20) Jud, W.; Vanzo, E.; Li, Z.; Ghirardo, A.; Zimmer, I.; Sharkey, T. D.; Hansel, A.; Schnitzler, J. P. Effects of Heat and Drought Stress on Post-Illumination Bursts of Volatile Organic Compounds in Isoprene-Emitting and Non-Emitting Poplar. Plant Cell and Environment **2016**, 39 (6), 1204–1215. https://doi.org/10.1111/PCE.12643.

(21) Kivimäenpää, M.; Riikonen, J.; Ahonen, V.; Tervahauta, A.; Holopainen, T. Sensitivity of Norway Spruce Physiology and Terpenoid Emission Dynamics to Elevated Ozone and Elevated Temperature under Open-Field Exposure. Environmental and Experimental Botany **2013**, 90, 32–42. https://doi.org/10.1016/J.ENVEXPBOT.2012.11.004.

(22) Kleist, E.; Mentel, T. F.; Andres, S.; Bohne, A.; Folkers, A.; Kiendler-Scharr, A.; Rudich, Y.; Springer, M.; Tillmann, R.; Wildt, J. Irreversible Impacts of Heat on the Emissions of Monoterpenes, Sesquiterpenes, Phenolic BVOC and Green Leaf Volatiles from Several Tree Species. Biogeosciences **2012**, 9 (12), 5111–5123. https://doi.org/10.5194/BG-9-5111-2012.

(23) Nagalingam, S.; Seco, R.; Kim, S.; Guenther, A. Heat Stress Strongly Induces Monoterpene Emissions in Some Plants with Specialized Terpenoid Storage Structures. Agricultural and Forest Meteorology **2023**, 333, 109400. https://doi.org/10.1016/J.AGRFORMET.2023.109400.

(24) Fitzky, A. C.; Kaser, L.; Peron, A.; Karl, T.; Graus, M.; Tholen, D.; Halbwirth, H.; Trimmel, H.; Pesendorfer, M.; Rewald, B.; Sandén, H. Same, Same, but Different: Drought and Salinity Affect BVOC Emission Rate and Alter Blend Composition of Urban Trees. Urban Forestry & Urban Greening **2023**, 80, 127842.

https://doi.org/10.1016/J.UFUG.2023.127842.

(25) Kivimäenpää, M.; Riikonen, J.; Valolahti, H.; Elina, H.; Holopainen, J. K.; Holopainen, T. Effects of Elevated Ozone and Warming on Terpenoid Emissions and Concentrations of Norway Spruce Depend on Needle Phenology and Age. Tree Physiology **2022**, 42 (8), 1570–1586. https://doi.org/10.1093/TREEPHYS/TPAC019.

(26) Braun, J.; Kaul, P.; Tost, R.; Witzler, M.; Carsten Engelhard, ·. Emission Dynamics of Constitutive and Herbivore-Induced Plant Volatiles from Norway Maple (Acer Platanoides) Trunk Infested by the Asian Longhorned Beetle (Anoplophora Glabripennis (Motschulsky)). Journal of Chemical Ecology 2026 52:3 **2026**, 52 (3), 46-. https://doi.org/10.1007/S10886-026-01718-2.

(27) Du, B.; Frühbrodt, T.; Delb, H.; Burzlaff, T.; Biedermann, P. H. W.; Kreuzwieser, J. Emission Patterns of Volatile Organic Compounds from Norway Spruce Logs Following Bark Beetle (Ips Typographus L.) Infestation. Tree Physiology **2025**, 45 (1). https://doi.org/10.1093/TREEPHYS/TPAE152.

(28) Brachmann, C. G.; Vowles, T.; Rinnan, R.; Björkman, M. P.; Ekberg, A.; Björk, R. G. Herbivore-Shrub Interactions Influence Ecosystem Respiration and Biogenic Volatile Organic Compound Composition in the Subarctic. Biogeosciences **2023**, 20 (19), 4069–4086. https://doi.org/10.5194/BG-20-4069-2023.

(29) Byron, J.; Pugliese, G.; de A. Monteiro, C.; Schuettler, J.; Edtbauer, A.; Gomes Alves, E.; Hartmann, S. C.; Tsokankunku, A.; Hall, D. H.; Dias-Junior, C. Q.; Harder, H.; Lelieveld, J.; Williams, J. Intense El Niño Provokes Production of New Reactive Volatiles as Stress Defences in Amazon Rainforest. Communications Earth & Environment **2026**, 7 (1), 419. https://doi.org/10.1038/s43247-026-03597-7.

(30) Jardine, K. J.; Jardine, A. B.; Holm, J. A.; Lombardozzi, D. L.; Negron-Juarez, R. I.; Martin, S. T.; Beller, H. R.; Gimenez, B. O.; Higuchi, N.; Chambers, J. Q. Monoterpene 'Thermometer' of Tropical Forest-Atmosphere Response to Climate Warming. Plant, Cell & Environment **2017**, 40 (3), 441–452. https://doi.org/10.1111/PCE.12879.

(31) Byron, J.; Pugliese, G.; Carolina, C. de; Robin, M.; Gomes Alves, E.; Schuettler, J.; Hartmann, S. C.; Edtbauer, A.; Krumm, B. E.; Zannoni, N.; Tsokankunku, A.; Dias-Junior, C. Q.; Quesada, C. A.; Harder, H.; Bourtsoukidis, E.; Lelieveld, J.; Williams, J. Mirror Image Molecules Expose State of Rainforest Stress. Communications Earth & Environment 2025 6:1 **2025**, 6 (1), 703-. https://doi.org/10.1038/s43247-025-02709-z.

(32) Dey, B.; Sjøgren, T. D.; Khare, P.; Gkatzelis, G. I.; Wu, Y.; Vasireddy, S.; Schultz, M.; Knohl, A.; Rinnan, R.; Hohaus, T.; Pfannerstill, E. Y. Multi-Stress Interaction Effects on BVOC Emission Fingerprints from Oak and Beech: A Cross-Investigation Using Machine Learning and Positive Matrix Factorization. Biogeosciences **2026**, 23 (4), 1423–1457. https://doi.org/10.5194/BG-23-1423-2026.

(33) Ferracci, V.; Bolas, C. G.; Freshwater, R. A.; Staniaszek, Z.; King, T.; Jaars, K.; Otu-Larbi, F.; Beale, J.; Malhi, Y.; Waine, T. W.; Jones, R. L.; Ashworth, K.; Harris, N. R. P. Continuous Isoprene Measurements in a UK Temperate Forest for a Whole Growing Season: Effects of Drought Stress During the 2018 Heatwave. Geophysical Research Letters **2020**, 47 (15), e2020GL088885. https://doi.org/10.1029/2020GL088885.

(34) Holopainen, J. K.; Gershenzon, J. Multiple Stress Factors and the Emission of Plant VOCs. Trends in Plant Science **2010**, 15 (3), 176–184. https://doi.org/10.1016/J.TPLANTS.2010.01.006.

(35) Zscheischler, J.; Westra, S.; Van Den Hurk, B. J. J. M.; Seneviratne, S. I.; Ward, P. J.; Pitman, A.; Aghakouchak, A.; Bresch, D. N.; Leonard, M.; Wahl, T.; Zhang, X. Future Climate Risk from Compound Events. Nature Climate Change **2018**, 8 (6), 469–477. https://doi.org/10.1038/S41558-018-0156-3.

(36) Qin, M.; She, Y.; Wang, M.; Wang, H.; Chang, Y.; Tan, Z.; An, J.; Huang, J.; Yuan, Z.; Lu, J.; Wang, Q.; Liu, C.; Liu, Z.; Xie, X.; Li, J.; Liao, H.; Pye, H. O. T.; Huang, C.; Guo, S.; Hu, M.; Zhang, Y.; Jacob, D. J.; Hu, J. Increased Urban Ozone in Heatwaves Due to Temperature-Induced Emissions of Anthropogenic Volatile Organic Compounds. Nature Geoscience **2025**, 18 (1), 50–56. https://doi.org/10.1038/S41561-024-01608.

(37) Dudareva, N.; Klempien, A.; Muhlemann, J. K.; Kaplan, I. Biosynthesis, Function and Metabolic Engineering of Plant Volatile Organic Compounds. New Phytologist **2013**, 198 (1), 16–32. https://doi.org/10.1111/NPH.12145.

(38) Pfannerstill, E. Y.; Reijrink, N. G.; Edtbauer, A.; Ringsdorf, A.; Zannoni, N.; Araújo, A.; Ditas, F.; Holanda, B. A.; Sá, M. O.; Tsokankunku, A.; Walter, D.; Wolff, S.; Lavri, J. V.; Pöhlker, C.; Sörgel, M.; Williams, J. Total OH Reactivity over the Amazon Rainforest: Variability with Temperature, Wind, Rain, Altitude, Time of Day, Season, and an Overall Budget Closure. Atmospheric Chemistry and Physics **2021**, 21 (8), 6231–6256. https://doi.org/10.5194/ACP-21-6231-2021.

(39) Coggon, M. M.; Stockwell, C. E.; Claflin, M. S.; Pfannerstill, E. Y.; Xu, L.; Gilman, J. B.; Marcantonio, J.; Cao, C.; Bates, K.; Gkatzelis, G. I.; Lamplugh, A.; Katz, E. F.; Arata, C.; Apel, E. C.; Hornbrook, R. S.; Piel, F.; Majluf, F.; Blake, D. R.; Wisthaler, A.; Canagaratna, M.; Lerner, B. M.; Goldstein, A. H.; Mak, J. E.; Warneke, C. Identifying and Correcting Interferences to PTR-ToF-MS Measurements of Isoprene and Other Urban Volatile Organic Compounds. Atmospheric Measurement Techniques **2024**, 17 (2), 801–825. https://doi.org/10.5194/AMT-17-801-2024.

(40) An, J.; Zhu, B.; Wang, H.; Li, Y.; Lin, X.; Yang, H. Characteristics and Source Apportionment of VOCs Measured in an Industrial Area of Nanjing, Yangtze River Delta, China. Atmospheric Environment **2014**, 97, 206–214. https://doi.org/10.1016/J.ATMOSENV.2014.08.021.

(41) Askari, A.; Chan, A. W. H. Volatile Organic Compound Emissions from a Multi-Unit Residential Building to Ambient Air. Environmental Science: Processes & Impacts **2025**, 27 (6), 1714–1730. https://doi.org/10.1039/D4EM00689E.

(42) Wernis, R. A.; Kreisberg, N. M.; Weber, R. J.; Drozd, G. T.; Goldstein, A. H. Source Apportionment of VOCs, IVOCs and SVOCs by Positive Matrix Factorization in Suburban Livermore, California. Atmospheric Chemistry and Physics **2022**, 22 (22), 14987–15019. https://doi.org/10.5194/ACP-22-14987-2022.

(43) Vestenius, M.; Hopke, P. K.; Lehtipalo, K.; Petäjä, T.; Hakola, H.; Hellén, H. Assessing Volatile Organic Compound Sources in a Boreal Forest Using Positive Matrix Factorization (PMF). Atmospheric Environment **2021**, 259, 118503. https://doi.org/10.1016/J.ATMOSENV.2021.118503.

(44) Wu, R.; Zorn, S. R.; Kang, S.; Kiendler-Scharr, A.; Wahner, A.; Mentel, T. F. Application of Fuzzy C-Means Clustering for Analysis of Chemical Ionization Mass Spectra: Insights into the Gas Phase Chemistry of NO3-Initiated Oxidation of Isoprene. Atmospheric Measurement Techniques **2024**, 17 (6), 1811–1835. https://doi.org/10.5194/amt-17-1811-2024.

(45) Niederbacher, B.; Winkler, J. B.; Schnitzler, J. P. Volatile Organic Compounds as Non-Invasive Markers for Plant Phenotyping. Journal of Experimental Botany **2015**, 66 (18), 5403–5416. https://doi.org/10.1093/jxb/erv219.

(46) Guenther, A. B.; Jiang, X.; Heald, C. L.; Sakulyanontvittaya, T.; Duhl, T.; Emmons, L. K.; Wang, X. The Model of Emissions of Gases and Aerosols from Nature Version 2.1 (MEGAN2.1): An Extended and Updated Framework for Modeling Biogenic Emissions. Geoscientific Model Development **2012**, 5 (6), 1471–1492. https://doi.org/10.5194/GMD-5-1471-2012.

(47) Guenther, A. B.; Zimmerman, P. R.; Harley, P. C.; Monson, R. K.; Fall, R. Isoprene and Monoterpene Emission Rate Variability: Model Evaluations and Sensitivity Analyses. Journal of Geophysical Research **1993**, 98 (D7), 12609–12617. https://doi.org/10.1029/93JD00527.

(48) Bourtsoukidis, E.; Pozzer, A.; Williams, J.; Makowski, D.; Peñuelas, J.; Matthaios, V. N.; Lazoglou, G.; Yañez-Serrano, A. M.; Lelieveld, J.; Ciais, P.; Vrekoussis, M.; Daskalakis, N.; Sciare, J. High Temperature Sensitivity of Monoterpene Emissions from Global Vegetation. Communications Earth & Environment 2024 5:1 **2024**, 5 (1), 23-. https://doi.org/10.1038/s43247-023-01175-9.

(49) Bourtsoukidis, E.; Guenther, A.; Wang, H.; Economou, T.; Lazoglou, G.; Christodoulou, A.; Christoudias, T.; Nölscher, A.; Yañez-Serrano, A. M.; Peñuelas, J. Environmental Change Is Reshaping the Temperature Sensitivity of Sesquiterpene Emissions and Their Atmospheric Impacts. Global Change Biology **2025**, 31 (6), e70258. https://doi.org/10.1111/GCB.70258.

(50) Düsseldorf, L. Düsseldorfer Zukunftsbaumliste; Düsseldorf, 2024. https://www.duesseldorf.de/fileadmin/Amt68/gartenamt/pdf/strassengruen/68_Br_Zukunftsbaumliste_komplett_A4_68s_screen_web_bf.pdf.

(51) Dorado, J. F.; Pinto, G.; Monteiro, P.; Chaves, N.; Alías, J. C.; Rodrigo, S.; Camisón, Á.; Solla, A. Heat Stress and Recovery Effects on the Physiology and Biochemistry of Castanea Sativa Mill. Frontiers in Forests and Global Change **2023**, 5, 1072661. https://doi.org/10.3389/FFGC.2022.1072661.

(52) Jaiswal, S.; Tripathi, D. K.; Gupta, R.; He, J.; Chen, Z. H.; Singh, V. P. Methyl-Salicylate: A Surveillance System for Triggering Immunity in Neighboring Plants. Journal of Integrative Plant Biology **2024**, 66 (2), 163–165. https://doi.org/10.1111/JIPB.13621.

(53) Martínez-Villa, J. A.; Paquette, A.; Feeley, K. J.; Morales-Morales, P. A.; Messier, C.; Durán, S. M. Changes in Morphological and Physiological Traits of Urban Trees in Response to Elevated Temperatures within an Urban Heat Island. Tree Physiology **2024**, 44 (12). https://doi.org/10.1093/TREEPHYS/TPAE145.

(54) Dusenge, M. E.; Duarte, A. G.; Way, D. A. Plant Carbon Metabolism and Climate Change: Elevated CO2 and Temperature Impacts on Photosynthesis, Photorespiration and Respiration. New Phytologist **2019**, 221 (1), 32–49. https://doi.org/10.1111/nph.15283.

(55) Guidi, L.; Degl'Innocenti, E. Ozone Effects on High Light-Induced Photoinhibition in Phaseolus Vulgaris. Plant Science **2008**, 174 (6), 590–596. https://doi.org/10.1016/J.PLANTSCI.2008.03.003.

(56) Mishra, S.; Heckathorn, S. A.; Barua, D.; Wang, D.; Joshi, P.; Hamilton, E. W.; Frantz, J. Interactive Effects of Elevated CO2 and Ozone on Leaf Thermotolerance in Field-Grown Glycine Max. Journal of Integrative Plant Biology **2008**, 50 (11), 1396–1405. https://doi.org/10.1111/j.1744-7909.2008.00745.x.

(57) Werner, C.; Fasbender, L.; Romek, K. M.; Yáñez-Serrano, A. M.; Kreuzwieser, J. Heat Waves Change Plant Carbon Allocation Among Primary and Secondary Metabolism Altering CO2 Assimilation, Respiration, and VOC Emissions. Frontiers in Plant Science **2020**, 11, 512788. https://doi.org/10.3389/FPLS.2020.01242.

(58) Jardine, K.; Elliott, A.; Seubert, H.; Kosina, S.; Pegoraro, E.; Crutchfield-Peters, K.; Brown, E.; Grasberger, E.; Benson, S.; Rinnan, R.; Torn, M.; Jardine kjjardine, K. Co-Variation of Declining Photosystem II Efficiency with Methyl Salicylate and Cis-β-Ocimene Emissions in Holcus Lanatus under High Light and Temperature. Discover Plants 2026 3:1 **2026**, 3 (1), 211-. https://doi.org/10.1007/S44372-026-00692-Z.

(59) Hakola, H.; Tarvainen, V.; Praplan, A. P.; Jaars, K.; Hemmilä, M.; Kulmala, M.; Bäck, J.; Hellén, H. Terpenoid and Carbonyl Emissions from Norway Spruce in Finland during the Growing Season. Atmospheric Chemistry and Physics **2017**, 17 (5), 3357–3370. https://doi.org/10.5194/acp-17-3357-2017.

(60) Yáñez-Serrano, A. M.; Fasbender, L.; Kreuzwieser, J.; Dubbert, D.; Haberstroh, S.; Lobo-Do-Vale, R.; Caldeira, M. C.; Werner, C. Volatile Diterpene Emission by Two Mediterranean Cistaceae Shrubs. Scientific Reports 2018 8:1 **2018**, 8 (1), 6855-. https://doi.org/10.1038/s41598-018-25056-w.

(61) Helin, A.; Hakola, H.; Hellén, H. Optimisation of a Thermal Desorption-Gas Chromatography-Mass Spectrometry Method for the Analysis of Monoterpenes, Sesquiterpenes and Diterpenes. Atmospheric Measurement Techniques **2020**, 13 (7), 3543–3560. https://doi.org/10.5194/AMT-13-3543-2020.

(62) Haberstroh, S.; Kreuzwieser, J.; Lobo-Do-Vale, R.; Caldeira, M. C.; Dubbert, M.; Werner, C. Terpenoid Emissions of Two Mediterranean Woody Species in Response to Drought Stress. Frontiers in Plant Science **2018**, 9, 373900. https://doi.org/10.3389/FPLS.2018.01071.

(63) Saito, T.; Kusumoto, N.; Hiura, T. Relation of Leaf Terpene Contents to Terpene Emission Profiles in Japanese Cedar (Cryptomeria Japonica). Ecological Research **2023**, 38 (1), 74–82. https://doi.org/10.1111/1440-1703.12323.

(64) Dorokhov, Y. L.; Sheshukova, E. V.; Komarova, T. V. Methanol in Plant Life. Frontiers in Plant Science **2018**, 871, 419877. https://doi.org/10.3389/FPLS.2018.01623.

(65) Jardine, K.; Karl, T.; Lerdau, M.; Harley, P.; Guenther, A.; Mak, J. E. Carbon Isotope Analysis of Acetaldehyde Emitted from Leaves Following Mechanical Stress and Anoxia. Plant Biology **2009**, 11 (4), 591–597. https://doi.org/10.1111/J.1438-8677.2008.00155.X.

(66) Nanaiah, G. K.; Anderson, J. A. Electrolyte Leakage and Evolution of Ethylene and Ethane from Pepper Leaf

Disks Following Temperature Stress and Fatty Acid Infiltration. J. AMER SOC. HORT. SCI **1992**, 117 (5), 846–851.

(67) Maeda, H.; Dudareva, N. The Shikimate Pathway and Aromatic Amino Acid Biosynthesis in Plants. Annual review of plant biology **2012**, 63, 73–105. https://doi.org/10.1146/ANNUREV-ARPLANT-042811-105439.

(68) Kanagendran, A.; Pazouki, L.; Li, S.; Liu, B.; Kännaste, A.; Niinemets, Ü. Ozone-Triggered Surface Uptake and Stress Volatile Emissions in Nicotiana Tabacum 'Wisconsin.' Journal of Experimental Botany **2018**, 69 (3), 681–697. https://doi.org/10.1093/JXB/ERX431.

(69) Tang, Y.; Zhong, L.; Wang, X.; Zheng, H.; Chen, L. Molecular Identification and Expression of Sesquiterpene Pathway Genes Responsible for Patchoulol Biosynthesis and Regulation in Pogostemon Cablin. Botanical Studies 2019 60:1 **2019**, 60 (1), 11-. https://doi.org/10.1186/S40529-019-0259-9.

(70) Fares, S.; Gentner, D. R.; Park, J. H.; Ormeno, E.; Karlik, J.; Goldstein, A. H. Biogenic Emissions from Citrus Species in California. Atmospheric Environment **2011**, 45 (27), 4557–4568. https://doi.org/10.1016/J.ATMOSENV.2011.05.066.

(71) Staudt, M.; Bertin, N.; Hansen, U.; Seufert, G.; Ciccioli, P.; Foster, P.; Frenzel, B.; Fugit, J. L. Seasonal and Diurnal Patterns of Monoterpene Emissions from Pinus Pinea (L.) under Field Conditions. Atmospheric Environment **1997**, 31 (SUPPL. 1), 145–156. https://doi.org/10.1016/S1352-2310(97)00081-2.

(72) Laffineur, Q.; Aubinet, M.; Schoon, N.; Amelynck, C.; Müller, J. F.; Dewulf, J.; Steppe, K.; Heinesch, B. Impact of Diffuse Light on Isoprene and Monoterpene Emissions from a Mixed Temperate Forest. Atmospheric Environment **2013**, 74, 385–392. https://doi.org/10.1016/J.ATMOSENV.2013.04.025.

(73) Hellén, H.; Praplan, A. P.; Tykkä, T.; Helin, A.; Schallhart, S.; Schiestl-Aalto, P. P.; Bäck, J.; Hakola, H. Sesquiterpenes and Oxygenated Sesquiterpenes Dominate the VOC (C5-C20) Emissions of Downy Birches. Atmospheric Chemistry and Physics **2021**, 21 (10), 8045–8066. https://doi.org/10.5194/ACP-21-8045-2021.

(74) Hansen, U.; Seufert, G. Temperature and Light Dependence of β-Caryophyllene Emission Rates. Journal of Geophysical Research: Atmospheres **2003**, 108 (24). https://doi.org/10.1029/2003JD003853.

(75) Nagalingam, S.; Wang, H.; Kim, S.; Guenther, A. Unexpectedly Strong Heat Stress Induction of Monoterpene, Methylbutenol, and Other Volatile Emissions for Conifers in the Cypress Family (Cupressaceae). Science of The Total Environment **2024**, 956, 177336. https://doi.org/10.1016/J.SCITOTENV.2024.177336.

(76) Vettikkat, L.; Miettinen, P.; Buchholz, A.; Rantala, P.; Yu, H.; Schallhart, S.; Petäjä, T.; Seco, R.; Männistö, E.; Kulmala, M.; Tuittila, E. S.; Guenther, A. B.; Schobesberger, S. High Emission Rates and Strong Temperature Response Make Boreal Wetlands a Large Source of Isoprene and Terpenes. Atmospheric Chemistry and Physics **2023**, 23 (4), 2683–2698. https://doi.org/10.5194/ACP-23-2683-2023.

(77) Pfannerstill, E. Y.; Arata, C.; Zhu, Q.; Schulze, B. C.; Ward, R.; Woods, R.; Harkins, C.; Schwantes, R. H.; Seinfeld, J. H.; Bucholtz, A.; Cohen, R. C.; Goldstein, A. H. Temperature-Dependent Emissions Dominate Aerosol and Ozone Formation in Los Angeles. Science **2024**, 384 (6702), 1324–1329. https://doi.org/10.1126/SCIENCE.ADG8204.

(78) He, X.; Yuan, B.; Huangfu, Y.; Gouw, J. de; Wang, S.; Yang, S.; Peng, Y.; Parrish, D. D.; Li, X.; Chang, M.; Mo, Z.; Min, K.-E.; Nam, W.; Chen, Y.; Zhang, X.; Qi, J.; Xie, Q.; Chen, W.; Guenther, A.; Wang, X.; Worsnop, D.; Karl, T.; Shao, M. Tree Selection in Urban Greening Shapes Air Quality for Global Cities. Science Advances **2026**, 12 (34), 5583. https://doi.org/10.1126/SCIADV.AEE5583.

(79) Hohaus, T.; Kuhn, U.; Andres, S.; Kaminski, M.; Rohrer, F.; Tillmann, R.; Wahner, A.; Wegener, R.; Yu, Z.; Kiendler-Scharr, A. A New Plant Chamber Facility, PLUS, Coupled to the Atmosphere Simulation Chamber SAPHIR. Atmospheric Measurement Techniques **2016**, 9 (3), 1247–1259. https://doi.org/10.5194/amt-9-1247-2016.

(80) Edtbauer, A.; Pfannerstill, E. Y.; Pires Florentino, A. P.; Barbosa, C. G. G.; Rodriguez-Caballero, E.; Zannoni, N.; Alves, R. P.; Wolff, S.; Tsokankunku, A.; Aptroot, A.; de Oliveira Sá, M.; de Araújo, A. C.; Sörgel, M.; de

Oliveira, S. M.; Weber, B.; Williams, J. Cryptogamic Organisms Are a Substantial Source and Sink for Volatile Organic Compounds in the Amazon Region. Communications Earth & Environment 2021 2:1 **2021**, 2 (1), 1–14. https://doi.org/10.1038/s43247-021-00328-y.

(81) Guenther, A. Isoprene Emission Estimates and Uncertainties for the Central African EXPRESSO Study Domain. Journal of Geophysical Research Atmospheres **1999**, 104 (D23), 30625–30639. https://doi.org/10.1029/1999JD900391.

(82) Yáñez-Serrano, A. M.; Peñuelas, J.; Jorba, O.; Graeffe, F.; Meder, M.; Garmash, O.; Zhang, Y.; Li, H.; Luo, Y.; Praplan, A.; Hellén, H.; Schobesberger, S.; Vettikkat, L.; Thomas, S.; Kurtén, T.; Taipale, D.; Bourtsoukidis, E.; Guenther, A.; Ehn, M. Unaccounted Impacts of Diterpene Emissions on Atmospheric Aerosol Loadings. Communications Earth & Environment 2025 6:1 **2025**, 6 (1), 636-. https://doi.org/10.1038/s43247-025-02613-6.

(83) Dey, B.; Depp, C.; Gu, Y.; Novelli, A.; Fuchs, H.; Hohaus, T.; Pfannerstill, E. Y. Data for: Climate-Stress VOC Fingerprints and Associated Stress-Dependent Temperature Sensitivity in Urban Trees (Linden, Chestnut). Jülich DATA **2026**. https://doi.org/10.26165/JUELICH-DATA/SSBSTP.

Supplementary Files

This is a list of supplementary files associated with this preprint. Click to download.

- SIFinalepbdep.pdf